Title	Assessing the predictions of a NOx kinetic mechanism on recent hydrogen and syngas experimental data
Author(s)	Zhang, Yingjia; Mathieu, Olivier; Petersen, Eric L.; Bourque, Gilles; Curran, Henry J.
Publication Date	2017-05-02
Publication Information	Zhang, Yingjia, Mathieu, Olivier, Petersen, Eric L., Bourque, Gilles, & Curran, Henry J. (2017). Assessing the predictions of a NOx kinetic mechanism on recent hydrogen and syngas experimental data. Combustion and Flame, 182, 122-141. doi: https://doi.org/10.1016/j.combustflame.2017.03.019
Publisher	Elsevier
Link to publisher's version	https://doi.org/10.1016/j.combustflame.2017.03.019
Item record	http://hdl.handle.net/10379/6874
DOI	http://dx.doi.org/10.1016/j.combustflame.2017.03.019

ASSESSING THE PREDICTIONS OF A NO$_X$ KINETIC MECHANISM ON RECENT HYDROGEN AND SYNGAS EXPERIMENTAL DATA

Yingjia Zhang[ab*], Olivier Mathieu[c], Eric L. Petersen[c], Gilles Bourque[d],

Henry J. Curran[b]

a. *State Key Laboratory of Multiphase Flow in Power Engineering, Xi'an Jiaotong University, Xi'an 710049, China.*
b. *Combustion Chemistry Centre, National University of Ireland, Galway, Ireland.*
c. *Texas A&M University, Department of Mechanical Engineering, College Station, TX, USA.*
d. *Siemens Canada Limited, 9545 Cote de Liesse Road, Montreal QC H9P 1A5, Canada*

Abstract

A detailed chemical kinetic mechanism has been developed to describe the pyrolysis and oxidation of the hydrogen/NO$_x$ and syngas/NO$_x$ systems. The thermodynamic data of nitrogenous compounds have been updated based on the study of Bugler et al. [J. Bugler, K.P. Somers, J.M. Simmie, F. Güthe, H.J. Curran. J. Phys. Chem. A, 2016, 120(36):7192–7197.]. The rate constants of individual elementary reactions associated with the Zeldovich mechanism, the N/O sub-mechanism (NO$_2$, N$_2$O and NO$_3$), the H/N/O sub-mechanism (HNO/HON, HNO$_2$/HONO and HONO$_2$) and the NH$_3$ mechanism (NNH and NH$_2$OH) have been selected through a synthetic comparison of the data available in the literature and the adoption of the latest available published rate constant data. The proposed mechanism has been validated against a large number of experimental data including pyrolysis histories, ignition delay time data, species profile versus time and temperature and flame speed measurements over a wide range of initial combustion conditions and various experimental devices including shock tubes, flow reactors, jet-stirred reactors and spherical combustion bombs.

The simulations of the proposed model have also been compared to those from five recently published kinetic models available in the literature. It was found that although these mechanisms generally reproduced well the data for which they were validated, they did not globally capture the combustion characteristics of all of the hydrogen/NO$_x$ and syngas/NO$_x$ systems.

Finally, the proposed model has been used to simulate the formation of NO at practical gas-turbine relevant conditions. A detailed flux analysis has been performed to kinetically explore the NO formation mechanism under various combustion conditions.

Keywords: NO$_x$ chemistry; Hydrogen; Syngas; Chemical kinetics; Model application

1. Introduction

Worldwide interest in emissions from gas turbine and internal combustion engines and the enactment of legislation to limit emissions has resulted in the need to understand the effect of exhaust emission control methods on engine performance [1]. Nitrogen oxides (NO_x), essentially the sum of nitric oxide (NO), nitrogen dioxide (NO_2) and nitrous oxide (N_2O), originate primarily from the oxidation of molecular nitrogen by the oxygen present in fuel/air mixtures at high temperatures ($T > 2100$ K). This is the so-called Zeldovich/Thermal NO_x mechanism. It is well known that in a diffusion flame combustor, the primary way to control thermal NO_x formation is to reduce the flame temperature in the combustor. To this end, over the past number of years, a large number of combustion technologies [2-7] have emerged to limit NO_x production during combustion. Nevertheless, it remains difficult to limit thermal NO_x formation to a zero level due to the presence of air in the reactant mixtures. Previous work suggests that even small amounts of nitrogen species can have a dramatic impact on fuel oxidation and combustion at low to high temperatures [8-12]. This effect is more noticeable in supersonic combustion tests where vitiated air streams are doped with NO_x species and can be introduced into the reaction chamber. Therefore, an advanced combustor design not only requires an understanding of the NO_x formation mechanisms, but also the exploration of the chemical interaction between the fuel and NO_x. For a hydrocarbon flame however, the interaction is reflected in part in Fenimore's prompt NO route *via* the reaction sequence $CH + N_2 = NCN + \dot{H}$ and $NCN + \dot{H}/\ddot{O}/\dot{O}H/O_2 = NO + CN/HCN/NCO$ [13, 14]. Ahmed et al. [15] indicated that a different subset of any available hydrocarbon mechanism can induce an obvious difference in the description of CH chemistry, leading to a significant effect on NO_x formation through

Fenimore's prompt mechanism. They also confirmed that for hydrogen and syngas combustion considerable uncertainty still remained in model predictions of both NO_x formation and the kinetic interaction between the fuel and NO_x species. It would appear that researchers have not come to a consensus with respect to a quantitative description of the interaction of NO_x with the free radical pool established, even by simple fuels such as hydrogen and syngas. In order to simplify the complexity of the reaction system, we have chosen the hydrogen/syngas/NO_x system as the target to omit the prompt-NO mechanism from the analysis enabling us to isolate and better expound the relative importance of the various NO_x formation routes such as the Zeldovich NO, the nitrous-oxide, the nitrous oxide and the NNH mechanism.

To investigate these processes at a more fundamental level, a number of studies involving the pyrolysis of N_2O and the oxidation of hydrogen/NO_x and syngas/NO_x have been performed in shock tubes [8, 16-27], jet-stirred reactors (JSR) [28-30], flow reactors (FR) [9, 10, 31, 32] and spherical expanding laminar flames [33, 34]. Simultaneously, many relative kinetic mechanisms [9, 10, 13, 28, 32, 35-43] have also been proposed to improve our understanding of NO_x formation and to develop NO_x control strategies. A very good review of nitrogen combustion chemistry before 1989 was carried out by Miller and Bowman [44] and only a brief summary based on recent publications is presented herein.

Glarborg et al. [32] conducted an experimental and theoretical work of impact of NO_x on moist CO oxidation under post-flame conditions ($p = 1.05$ atm, $T = 800 - 1400$ K, $x_{NO} = 0 - 1\%$, and $x_{NO_2} = 0 - 622$ ppm). The concentrations of the major species including CO, CO_2, NO and NO_2 were measured and used for model development. The rate constants for the NO_x subset were mainly adopted from the recommendations of Tsang and Herron [38] and updated portions of rate constants

using literature recommendations, mainly including radical recombination reactions, NO formation recycled by reactions of HNO, NO_2, HONO and NO_3 with chain carriers. The model showed a general good agreement with the data. Glarborg et al. [32] pointed out that the presence of NO and NO_2 significantly affects CO consumption. In particular, NO represented a two-fold impact with respect to CO oxidation at lower temperatures through 1) enhancing CO consumption by converting $H\dot{O}_2$ radicals into $\dot{O}H$ radicals *via* the reaction $NO + H\dot{O}_2 = NO_2 + \dot{O}H$ at low NO concentrations and 2) inhibiting CO consumption by catalyzing chain-carrier recombination *via* $\dot{O}H/\dot{H}/\ddot{O} + NO\ (+M) = HONO/HNO/NO_2\ (+M)$. In contrast, NO_2 was observed to be more efficient in scavenging reactive radicals. However, in the shock tube measurements, the experimental observations showed the opposite effect of NO_2 with either hydrogen [8] or a hydrocarbon fuel [45], because of the higher temperatures (> 1400 K) relative to the flow reactor experiments (600 – 1400 K).

To further supplement early atmospheric-pressure flow reactor studies [32, 46, 47], Mueller et al. [10] conducted an experimental and modeling study of H_2/O_2 and $CO/H_2O/O_2$ reaction kinetics in the presence of trace quantities of NO and NO_2 at conditions relevant to auto-ignition and post-combustion expansion processes ($p = 0.5 - 14$ atm, $T = 750 - 1100$ K, $\varphi = 0.25 - 1.0$, $x_{NO} = 12 - 532$ ppm, and $x_{NO_2} = 85$ ppm). This work confirmed the experimental observations of Glarborg et al. [32] and also clarified the fact that the effect of the addition of NO on fuel oxidation and NO to NO_2 conversion not only depends strongly on NO concentration but also depends on pressure and on equivalence ratio. The inter-conversion of NO with NO_2 can consume H_2 and CO at much lower temperatures relative to that which occurs in the absence of NO_x species. The measurements of the concentrations of H_2, CO, O_2, H_2O, CO_2, NO, NO_2 HONO and temperature

were used to develop a detail kinetic mechanism which was capable of reproducing their experimental measurements.

Konnov et al. [48, 49] constructed a detail H/N/O mechanism to computationally investigate the NO production rate for fuel-lean, stoichiometric and fuel-rich hydrogen/air reaction systems in well-stirred reactors over a temperature range of $1500 - 2200$ K. They clarified the validity of steady-state assumptions used in the development of explicit expressions used to predict the instantaneous NO formation rate in a hydrogen flame at residence times of $1 - 25$ ms. Furthermore, Konnov et al. identified a possible new route to NO formation in fuel-rich hydrogen combustion *via* a sequence of reactions relating to N_2H_3 radicals, and also emphasized the importance of NNH chemistry to form NO that was first proposed by Bozzelli and Dean [50]. Subsequently, Konnov [13] released a revised model with an update of an additional implementation of kinetic pathways to prompt-NO formation *via* NCN chemistry.

Dayma and Dagaut [28] explored the oxidation of a diluted hydrogen system perturbed with various concentrations of NO and NO_2 at typical JSR conditions ($p = 1.0 - 10$ atm, $T = 700 - 1150$ K, $\varphi = 0.1 - 2.5$, $x_{NO} = 220 - 250$ ppm, and $x_{NO_2} = 65 - 70$ ppm). They proposed a detailed kinetic model to interpret their experimental data and indicated that the mutual sensitization effect of NO and/or NO_2 on hydrogen oxidation can be attributed to 1) the conversion of unreactive $H\dot{O}_2$ radicals into reactive $\dot{O}H$ radicals *via* the reaction $NO + H\dot{O}_2 = NO_2 + \dot{O}H$ which promotes hydrogen oxidation *via* $H_2 + \dot{O}H = H_2O + \dot{H}$, and 2) the recycled generation of NO *via* $NO_2 + \dot{H} = NO + \dot{O}H$ together with the release of $\dot{O}H$ radicals. Moreover, the sensitization of relative importance reflected by these reactions presented a different pressure dependence in the range $1 - 10$ atm. Unfortunately,

the Dayma and Dagaut model disagreement significantly with the ignition delay times of $H_2/O_2/NO_2$ reported by Slack and Grillo [51].

Rasmussen et al. [9] conducted a well-defined experimental investigation of homogeneous $CO/H_2/O_2/NO_x$ mixtures in a high-pressure laminar flow reactor at the following conditions: $p = 20 -$ 100 atm, $T = 600 - 900$ K, $\varphi = 0.063$, $x_{NO}/x_{NO_2} = 36/113$ ppm, 125/26 ppm and 145/6 ppm corresponding to 20, 50 and 100 atm, respectively. The concentrations of major species, CO, CO_2, O_2, NO and NO_2, were recorded. Furthermore, a detailed kinetic model was proposed with updated rate constants and thermodynamic properties using either *ab initio* CBS-QBS calculations or new literature recommendations. The model reproduced the species histories for $H_2/CO/O_2/NO_x$ oxidation at high pressures pretty well, and was in reasonable agreement with literature flow reactor data, but trended to over-predict the reactivity of syngas ignition.

Mathieu et al. [8, 18] assessed the validity of both the H_2/O_2 chemistry and NO_x sub-mechanisms incorporated respectively in the literature models [9, 13, 28] against their own measured ignition delay times. The simulations showed that, although these models were in part in reasonable agreement with the new data for the $H_2/O_2/NO_x$ system, none of them could reproduce correctly the ignition trend for the neat H_2/O_2 system. Ahmed et al. [15] and Watson et al. [52] found that the discrepancy of the NO_x subset was particularly more important in predicting species evolution at high-pressure flow reactor conditions.

Considering the shortcomings of the mechanisms [9] used by Mathieu et al. [8, 18] to simulate their pure H_2/O_2 system, most recently Ahmed et al. [15] proposed a detailed mechanism to describe $H_2/CO/NO_x$ oxidation. They integrated the literature NO_x reaction schemes [9, 13, 28, 49, 53] with the H_2/O_2 reaction scheme published by Burke et al. [54]. They also updated several of the rate

constants for reactions recommended by Klippenstein et al. [39] relating to the NH_2, HNO and NH_2OH species. The assembled model generally showed a reasonable agreement with recent experimental data measured in various facilities including a shock tube, a FR and a JSR over a wide range of conditions. Nevertheless, the model still over-predicted the ignition delay times reported by Mathieu et al. [8] even considering $\dot{H}$ atom impurity condensation, especially more notably at high pressures and high NO_2 levels. We have therefore re-evaluated the Burke et al. [54] model against recent data measured by Hashemi et al. [55] in a high-pressure FR for neat $H_2/O_2/N_2$ mixtures. Results show that the Burke et al. model presents slow H_2 consumption at $800 - 900$ K, and the deviation tends to be more dramatic transitioning from fuel-rich to fuel-lean mixtures, see Fig. S1 of the Supplementary material.

Extensive kinetic modeling studies have been carried out for hydrogen/NO_x and syngas/NO_x combustion. Such studies however, have not systematically addressed the combined effects of all of the reactions. In fact, each individually recommended rate constant and species thermochemistry have an associated uncertainty, which can propagate through the complete model and can eventually produce an undesirable simulation result [56]. With this in mind, the aim of *this study* is 1) to evaluate the effect of important reactions on the kinetic interaction of the hydrogen/syngas sub-mechanism with the NO_x subset at different physical operating conditions (ambient temperature, ambient pressure, equivalence ratio, and concentrations of NO_x); 2) to develop a mechanism with significant updates based on recent thermodynamic and kinetic data. The aim is to produce a model capable of reproducing the combustion characteristics of both neat hydrogen/syngas and hydrogen/syngas/NO_x systems over a wide range of experimental targets and conditions measured using shock tube pyrolysis data, ignition delay times, JSR species profiles, laminar and turbulent FR

speciation data and flame speeds; and 3) to attempt to provide a promising strategy controlling NO formation through a preliminary kinetic exploration of NO at practical gas-turbine conditions. We expect that the model can be predictive in nature with the ultimate goal of advancing the design and optimization of practical fuel-flexibility engine systems to control NO_x formation.

2. Mechanism development

2.1. Thermochemistry

As mentioned above, erroneous or inconsistent use of both chemical kinetic and thermochemical data may result in a series of compensating errors which may result in an eventual good prediction of a limited number of targets. To avoid possible uncertainties stemming from thermochemistry, an accurate and consistent set of thermodynamic data is certainly necessary. In *this study*, thermodynamic data for hydrogen, carbon monoxide and related radicals are adopted from the NUI Galway hydrogen/syngas mechanism [57]. Moreover, thermodynamic data of nitrogen-containing compounds are taken from the recent work of Bugler et al. [58], where a new gas-phase thermochemistry database was calculated using high-level *ab* initio calculations for 60 nitrogenous compounds that exist in practical combustion environments. Three quantum-chemical compound methods (CBS-APNO, G3 and G4) were used to derive heats of formation, while the B3LYP/cc-pVTZ level of theory was used to calculate entropies and heat capacities. Simulated results showed that the thermochemistry database presented a decrease of 10% and 20% in NO and N_2O concentrations, respectively, and an increase of 20% in the concentration of NO_2 compared to literature data. However, Bugler et al. reported the deviation archives to be approximately a factor of three for some important intermediates such as HONO and HNO_2.

As we mentioned above, the coupled nature of the kinetics and the thermochemistry can impact on modeling results. To clarify the effect of thermochemistry, we have combined our current kinetic model with the thermochemical parameters from difference sources (Ahmed_2016 [15], Konnov_2009 [13], SJK/PG_2015 [31, 39], Mével_2009 [19]. and Dagaut_2008 [59]), to simulate common targets including ignition delay times (Fig. 1), FR speciation (Fig. 2), and JSR species concentrations (Fig. 3).

For ignition delay times the impact of thermochemistry is generally limited at low pressures, Fig. 1. At high pressures, however, the effect becomes more prominent, particularly at lower temperatures (< 1150 K). The simulations using the Ahmed et al. thermochemistry are consistent with those predicted by our model and both are in excellent agreement with the experiments. In contrast, the other three are similar to the data but slightly over-predict the ignition delay times.
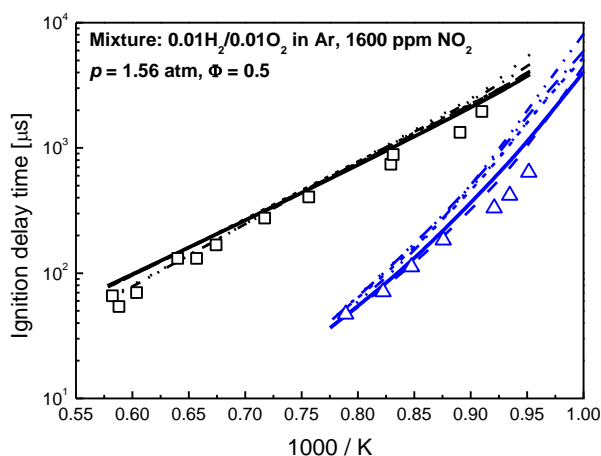

Fig. 1. Effect of choice of thermochemistry on ignition delay time simulations at typical shock tube conditions. Symbols represent Mathieu et al. [8] measurements. Lines denote model simulations with the current model (solid line), Ahmed_2016 [15] (dash line), Konnov_2009 [13] (dot line), SJK/PG _2015 [31, 39] (dash dot line), Mével_2009 [19] (dash dot dot line) and Dagaut_2008 [59] (short dash line).

For FR species versus time prediction, likewise, the thermochemistry has a limited impact at low pressures but it is significant at higher pressures, Fig. 2. Specifically, the thermochemistry in current model, Ahmed_2016, SJK/PG_2015 and Dagaut_2008 show almost the same predictions of the concentrations of the major species, and they are also in very good agreement with the Mueller et al. measurements. [10]. The thermochemistry from Konnov_2009 and Mével_2009 present an obvious deviation, particularly at late stages of oxidation (> 0.5 s) where these two data sets lead to a slow prediction of the consumption of the fuel and formation of NO relative to the experiments.
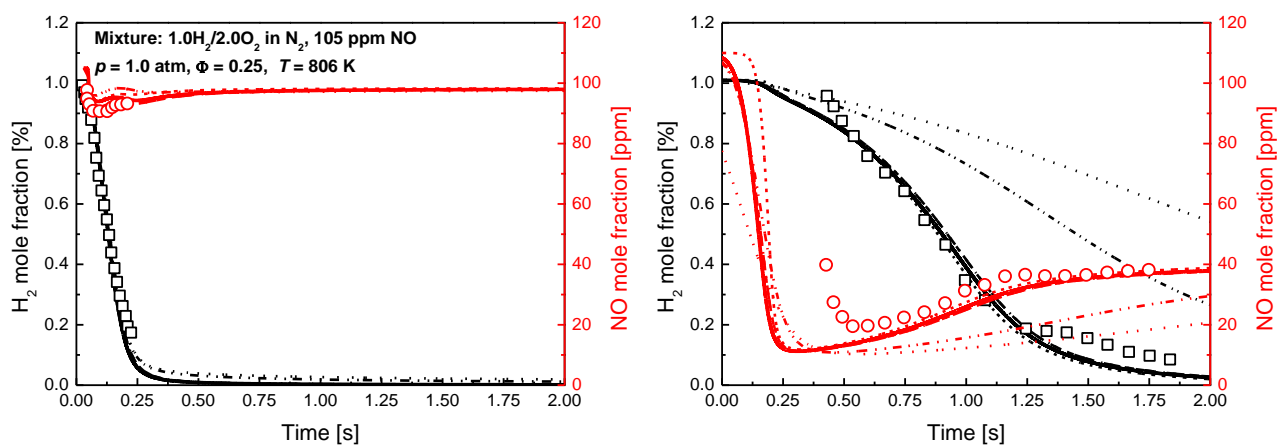

Fig. 2. Effect of thermochemistry on simulating the oxidation of hydrogen/NOx at typical flow reactor conditions. Symbols represent Mueller et al. [10] measurements. Lines denote model simulations with the current model (solid line), Ahmed_2016 [15] (dash line), Konnov_2009 [13] (dot line), SJK/PG _2015 [31, 39] (dash dot line), Mével_2009 [19] (dash dot dot line) and Dagaut_2008 [59] (short dash line).

In contrast, the effect of thermochemistry is fairly remarkable in the prediction of hydrogen/NOx oxidation in a JSR, even at low pressure. At 1.0 atm, Fig. 3(a), the difference in thermochemistry has a negligible effect on the evolutions of both the hydrogen and water profiles but has a dramatic effect on NO to NO_2 conversion. It is clear that the thermochemistry from Dagaut_2009 and SJK/PG did not improve NO formation at higher temperatures (> 850 K), while the other sets are in good agreement with the measurements [28]. At high pressures (10 atm), the conversion of NO to

NO2 is reproduced well by all data sets for all conditions whereas using the data of Konnov_2009

and Mével_2009 result in slow predictions in Ḣ atom conversion from hydrogen to water at 800 −
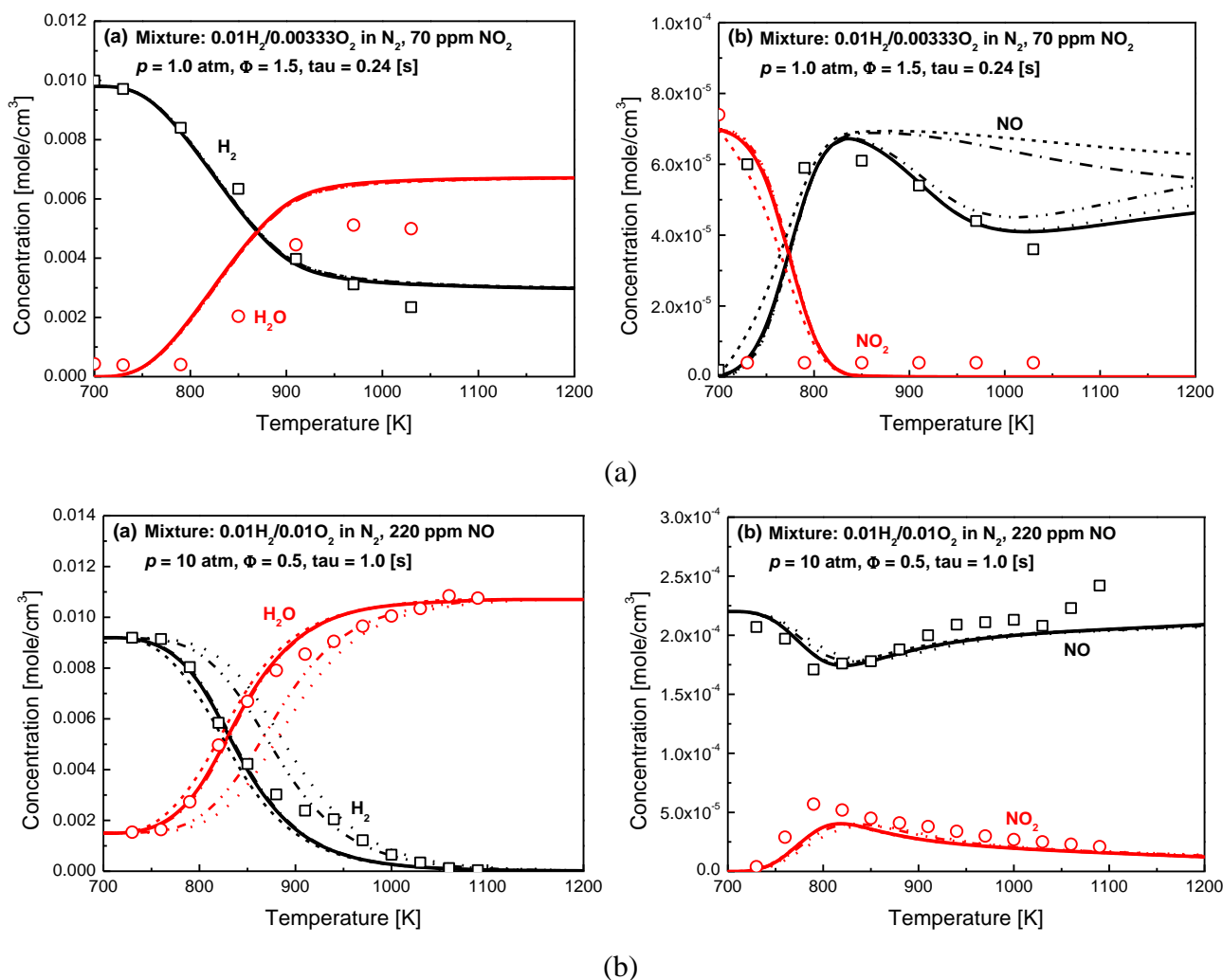
1100 K, Fig. 3(b).

(a)

(b)

Fig. 3. Effect of thermochemistry on simulating oxidation of hydrogen/NOx at typical JSR conditions. Symbols represent Dayma and Dagaut experiments [28]. Lines denote model simulations with the current model (solid line), Ahmed_2016 [15] (dash line), Konnov_2009 [13] (dot line), SJK/PG _2015 [31, 39] (dash dot line), Mével_2009 [19] (dash dot dot line) and Dagaut_2008 [59] (short dash line). (a) Low pressure (1.0 atm); (b) high pressure (10 atm).

It is clear that the choice of thermochemistry does effect model simulations and that different

sources result in different simulated results for commonly validated targets. Overall, simulations

using the thermochemistry adopted here are in good agreement with that using the data from Ahmed et al. [15] and the experimental measurements as well.

2.2. Kinetic reaction mechanism

The proposed kinetic mechanism of hydrogen/NO_x and syngas/NO_x is developed upon the mechanism of hydrogen and syngas to hierarchically incorporate the sub-sets such as the Zeldovich mechanism, the N/O and H/N/O schemes and an NH_3 sub-mechanism, which are important to describe NO_x formation and its interaction with hydrogen and syngas. The complete kinetic mechanism is available as Supplementary material.

2.2.1 H₂/syngas sub-mechanism

Similar to the selection of thermochemistry data, the sub-mechanism of H_2/CO is adopted from the work of Kéromnès et al. [57] with updates of several critical reactions based on recent experimental and theoretical data. This model has been validated widely using ignition delay times measured in both shock tubes and rapid compression machines, speciation data in both JSRs and FRs, laminar flame speeds, and mass burning rates.

2.2.2 HOĊO radical chemistry

Due to the consideration of HOĊO chemistry in terms of the kinetic importance of the conversion of CO to CO_2 in combustion environments, HOĊO related reactions were added in the Kéromnès H_2/CO/O_2 mechanism. Recently, Barker's group [60, 61] applied *ab initio* Semi-Classical Transition State Theory (SCTST) to calculate the limiting low- and high-pressure rate coefficients for HOĊO unimolecular dissociation reactions. The thermal rate constants calculated were in reasonable agreement with literature experimental data, and have been adopted in the current model.

For bimolecular reactions of HOĊO, Yu et al. conducted a series of quantum chemical calculations using an *ab initio* direct dynamics method for the reactions of HOĊO + O_2 [62], HOĊO + ȮH [63], HOĊO + Ḣ [64], HOĊO + Ö [65], HOĊO + HȮ$_2$ [66] and HOĊO + ĊH$_3$ [67]. For consistency, all of the rate constants of HOĊO with free radicals are taken from Yu et al., including those provided in their recent review [68]. Moreover, the reactions of HOĊO + NO/NO$_2$ are adopted from the theoretical calculations of Poggi et al. [69, 70].

Fig. 4 shows the effect of HOĊO chemistry on the conversion of CO to CO_2 in the H_2/CO/NO$_x$ reaction system at high pressures. Clearly, the new HOĊO reaction pathways promote the conversion of CO to CO_2 at temperatures above 700 K, whereas there is a negligible effect on NO$_x$ formation. In fact, the conversion of NO to NO_2 at these conditions is most sensitive to the reactions: NO + Ö (+M) = NO_2 (+M) and NO + O_2 = NO_2 + Ö, but it is not influenced by the HOĊO chemistry. Note that the promoting effect of HOĊO chemistry appears to be only important at high pressure ($p > 50$ atm), while it is much more limited at lower pressures ($p < 20$ atm).

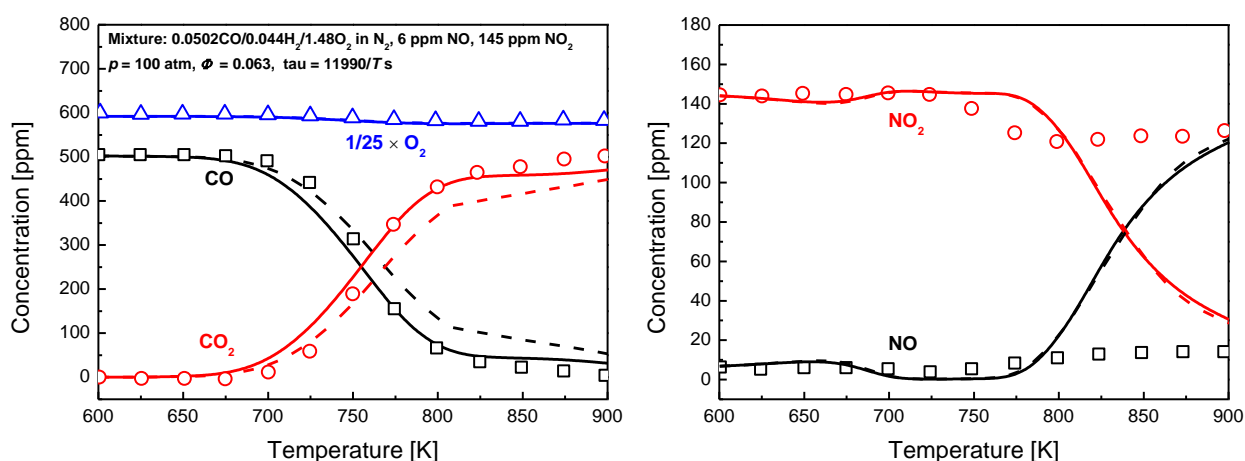Fig. 4. Effect of HOĊO chemistry on CO to CO_2 conversion in the H_2/CO/O_2/NOx reaction system at high pressures. Symbols represent flow reactor experimental measurements [9]; lines denote model predictions with HOĊO chemistry (solid line) and without HOĊO chemistry (dash line) at isothermal assumption.

2.2.3 Zeldovich mechanism

Thermal NO_x is an important source of NO formation in combustors at high temperatures. The kinetic formation process has been well characterized in the Zeldovich mechanism [71] namely:

$$\ddot{O} + N_2 = NO + N \quad \text{R1}$$

$$N + O_2 = NO + \ddot{O} \quad \text{R2}$$

$$N + \dot{O}H = NO + \dot{H} \quad \text{R3}$$

Due to the importance of the rate-limiting step, R1, Baulch et al. [72] reviewed the measurements of the rate constant of R1, and recommended a temperature-independent value of $k{-}1$ of 2.1×10^{13} cm^3 mol^{-1} s^{-1} and this rate constant has been widely used in most NO_x kinetic mechanisms [9, 13, 15, 29, 39, 53, 73]. Nevertheless, the recent experiments reported by Abian et al. [31] indicated that adopting the rate constant recommended by Baulch et al. leads to an under-prediction of thermal NO formation, especially in the presence of high concentrations of O_2. In contrast, using the Abian et al. rate constant shows excellent agreement with their own experimental data as well as with the literature data [17]. Therefore, we have adopted the recommendation of Abian et al. [31] to describe R1. Moreover, the rate constant of R2 is taken from Baulch et al. [36] since it is in excellent agreement with experimental literature data [74-77], while the rate constant of R3 is taken from the recommendation of Miller et al. [44, 78], which is consistent with the direct measurement of Howard and Smith [79].

2.2.4 N/O sub-mechanism

Overall, the N/O sub-mechanism consists of four chemical species, namely nitric oxide (NO), nitrogen dioxide (NO_2), nitrous oxide (N_2O) and nitrogen trioxide (NO_3). Owing to fact that NO acts

to either eliminate free radicals to form stable species *via* recombination reactions, or it acts as a chain carrier, participating in other reactions of nitrogenous compounds. The NO scheme will be thus discussed along with above the four N/O schemes.

2.2.4.1 NO_2 scheme

NO_2 is initially formed *via* the recombination reaction between NO and Ö atom,

$$NO + \ddot{O} \ (+M) = NO_2 \ (+M) \quad \text{R4}$$
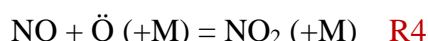
The rate constant of R4 is taken from the recommendation by Tsang and Herron [38]. The low- and high-pressure limits of R4 were derived, and were shown to be in good agreement with measurements. Third body collision efficiencies are adopted from Baulch et al. [72]. Considering the impact of the low pressure limit (LPL) on the consumption of CO under flow reactor conditions, we have increased the A-factor of the LPL by a factor of two which is within the uncertainty of a factor of three suggested by Tsang and Herron to better reproduce the CO species consumption profiles measured in a flow reactor.

NO_2 is mainly formed/consumed by reacting with either free radicals:

$$NO_2 + \dot{H} = NO + \dot{O}H \quad \text{R5}$$

$$NO_2 + \ddot{O} = NO + O_2 \quad \text{R6}$$

$$NO_2 + \dot{O}H = NO + H\dot{O}_2 \quad \text{R7}$$

$$NO_2 + H\dot{O}_2 = HONO/HNO_2 + O_2 \quad \text{R8}$$

or with fuels, namely H_2 and CO in the current work.

$$NO_2 + H_2 = HONO/HNO_2 + \dot{H} \quad \text{R9}$$

$$NO_2 + CO = NO + CO_2 \quad \text{R10}$$

The importance of R5 and R−7 with respect to inter-conversion of NO to NO_2 and accumulation of $\dot{O}H$ radicals was identified in many reaction systems [8-10, 28, 45]. In *this study*, we have adopted the rate constants of R5 measured directly by Ko and Fontjin [80] which is close to the Baulch et al. [72] recommendation within an uncertainty by a factor of two. In order to accurately predict the species data from Mueller et al. [10] we have made a small (20%) adjustment in this rate constant which is well within the uncertainty limit mentioned above. The rate constant of R−7 is taken from Baulch et al. [72] evaluation based largely on experimental sets, and it is generally in good agreement with Howard [81] measurement and Tsang and Herron [38] recommendation. The rate constant of R6 is adopted from Tsang and Herron [38] recommendation due to its consistency with the experimental measurements [82-85] and high-level quantum chemistry calculation [86]. Glarborg et al. [87] in their study of the interaction of formaldehyde with NO_x found that R8 can compete with the reaction of $H\dot{O}_2 + H\dot{O}_2 = H_2O_2 + O_2$ and R−7 for $H\dot{O}_2$ radicals, limiting the concentration of NO_2. Rasmussen et al. [9] performed an *ab initio* study at the CBS-QB3 level of theory and clarified that the channel forming $HNO_2 + O_2$ dominates at typical combustion conditions. Here, we have adopted the rate constant of Rasmussen et al. [9] for R8. As proposed by Mathieu et al. [8], R9 plays a role in their brute force sensitivity analysis. However, previous modeling studies [10, 13, 29] rarely distinguish the HNO_2 isomer (*cis*-HONO, *trans*-HONO and HNO_2) as the products of R9. Considering the lack of consensus regarding the rate constants for the channel forming the HNO_2 isomers, Chai and Goldsmith [40] conducted a high-accuracy electronic structure calculation on the rate constants. Their results show that, although *trans*-HONO represents the most stable state, the dominant product is *cis*-HONO, followed by HNO_2. The total rate of R8 calculated by Chai and Goldsmith is in excellent agreement with that reported both in the Park et al. [88] measurement and

the Rasmussen et al. [9] calculation, but it is an order of magnitude lower than the Tsang and Herron [38] recommendation. Here, we use the Chai and Goldsmith [40] calculations for R9. Fortunately, there appears to be little or no disagreement in the literature [38, 89, 90] in the recommended rate constant of R10. We have assigned the Tsang and Herron [38] recommendation for this reaction.
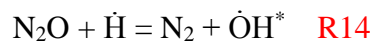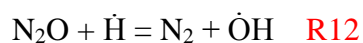
2.2.4.2 N_2O scheme

The N_2O mechanism can be important in high pressure flames or under fuel-lean conditions at low temperatures. Indeed, N_2O is primarily formed *via* the recombination reaction of molecular nitrogen with Ö atoms (R11), while its decomposition can also play a role in the release of active Ö atoms at low pressures.

$$N_2 + Ö \ (+M) = N_2O \ (+M) \quad \text{R11}$$
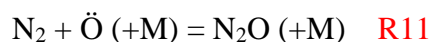
Mathieu et al [18] indicated that an increase in reactivity can be attributed to the additional Ö atoms released *via* R−11, as the Ö atoms produced are free to undergo chain branching through the reaction of $H_2 + Ö = Ḣ + ȮH$. Javoy et al. [20] experimentally determined the LPL of R−11 with an overall uncertainty of less than 18%. Their result are in good agreement with both the experimental measurements [91-93] and with the theoretical determination [94]. Moreover, Javoy et al. [20] adopted the high pressure limit (HPL) rate constant from Zuev and Starikovskii [95] for R−11 as the activation energy was consistent with the calculation of Chang and Yarkon [94]. Here, we select the Javoy et al. recommended expression in our model since the rate constant leads to a better prediction in both N_2O decomposition and ignition delay time measurements. The third body efficiencies of the R−11 are taken from Konnov [13].

In a similar manner to the NO_2 scheme discussed above, N_2O is also mainly consumed by free radical attack *via* the following sequence of reactions:

$$N_2O + \dot{H} = N_2 + \dot{O}H \quad \textcolor{red}{R12}$$

$$N_2O + \dot{H} = NH + NO \quad \textcolor{red}{R13}$$

$$N_2O + \dot{H} = N_2 + \dot{O}H^* \quad \textcolor{red}{R14}$$

$$N_2O + \ddot{O} = N_2 + O_2 \quad \textcolor{red}{R15}$$

$$N_2O + \ddot{O} = NO + NO \quad \textcolor{red}{R16}$$

$$N_2O + \dot{O}H = N_2 + H\dot{O}_2 \quad \textcolor{red}{R17}$$

$$N_2O + \dot{O}H = HNO + NO \quad \textcolor{red}{R18}$$

$$N_2O + NO = NO_2 + N_2 \quad \textcolor{red}{R19}$$

$$N_2O + H_2 = N_2 + H_2O \quad \textcolor{red}{R20}$$

Using both sensitivity and flux analyses the reaction of N_2O with $\dot{H}$ atoms (R12) has been highlighted as the primary reaction channel in predicting laminar flame speed and energy release predictions in H_2/N_2O flames [33] and is the second most important reaction for ignition delay time predictions [96]. Marshall et al. [97] and Baulch et al. [72] determined the rate constant for R12 with a non-typical Arrhenius dependence with temperature. However, a more recent study of Klippenstein et al. [39] did not support the hypothesis that the change in activation energy in the low-temperature Arrhenius plot is due to a tunneling effect through an Eckart potential barrier as suggested by Marshall et al. [97], but is instead due to stabilization in the potential energy wells of *cis*- and *trans*-HNNO. Together, they found that the reactions of R12 and R13 are to be essentially pressure-independent, at least up to 1 atm. In fact all of the aforementioned studies [39, 72, 97] are in relatively close agreement. In *this study*, we have adopted the most recent calculations from

Klippenstein et al. [39] to describe R12 and R–13. Considering the effect of excited hydroxyl radicals (OH[*]) on the simulation of N_2O ignition times suggested by Mével et al. [96] and Mathieu et al. [18], we take the rate constant of R14 from the measurement of Hidaka et al. [24] which is in good agreement with the formation of OH[*] measured in their N_2O/H_2 system in the temperature range 1400 – 2000 K. Dean and Bozzelli [98] reviewed literature data [38, 44, 91, 93, 99] and found that most experiments were in good agreement for the rate constant of R16 whereas there was a considerable discrepancy in the rate constant for R15. In order to provide reliable information to interpret the deviations for R15 present in most of the previous studies, Meagher and Anderson [100] critically evaluated these literature data using detailed chemical modeling in terms of the product channels and confirmed the reliability of the rate constant of R15 measured by Davidson et al. [99]. Together, Meagher and Anderson also proposed a rate constants for R16 through combining the literature data with their direct measurements [101]. In this model, we have selected the rate constants resulting from the intensive study of Meagher and Anderson [100] and are also recommended by Baulch et al. [72] for R15 and R16. Moreover, Mebel et al. [102] calculations using TST and RRKM theories are adopted for R17-R19, while Kosarev et al. estimation is chosen to for R20.
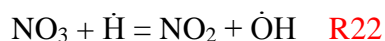
2.2.4.3 NO_3 scheme

NO_3 is initially formed by the recombination of NO_2 with Ö atoms *via* the following reaction:

$$NO_2 + Ö (+M) = NO_3 (+M) \quad \text{R21}$$
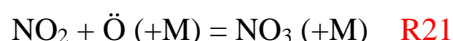
Clearly, R21 competes with R6 for Ö atoms, such that the ratio of the rate constants for R6 and R21 is important in determining the formation and consumption of NO_2. As mentioned by Hahn et al.

[103], the reaction R21 may involve the same intermediate, similar to $H\dot{O}_2$ radicals in the reactions $\dot{H}$ + O_2 = $\ddot{O}$ + $\dot{O}H$ and $\dot{H}$ + O_2 (+M) = $H\dot{O}_2$ (+M). Hahn et al. measured the absolute rate for the sum of R6 and R21 over a wide range of pressure (1 − 900 bar). Meanwhile, they also theoretically calculated the HPL for R21 based on the Harding et al. [104] trajectory calculation approach, and the results are in agreement with the experimental data within a factor of two. Considering the fact that a small uncertainly in the rate constant of R6 can result in a large uncertainty in the LPL of R21, we use the rate constants determined by Hahn et al. [103] for R21 in order to be internally consistent because the same rate constant for R6 were used in our model and in that of Hahn et al.

Unlike NO_2 and N_2O, NO_3 mainly undergoes O-atom abstraction by free radicals *via* the following reaction sequence to convert to NO_2.

$$NO_3 + \dot{H} = NO_2 + \dot{O}H \quad \text{R22}$$

$$NO_3 + \ddot{O} = NO_2 + O_2 \quad \text{R23}$$

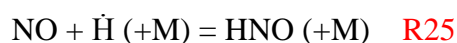$$NO_3 + \dot{O}H = NO_2 + H\dot{O}_2 \quad \text{R24}$$

Reactions 22–24 presented above do not appear to be important at combustion conditions and their rate constants have been adopted from the recommendations of Atkinson et al. [105] and Becker et al. [106] in this model.

2.2.5 H/N/O sub-mechanism

The H/N/O sub-mechanism essentially consists of five chemical species, namely nitroxyl (HNO), HON, nitrous acid isomers ($HONO/HNO_2$), and nitric acid isomers ($HONO_2$).

2.2.5.1 HNO scheme

The closed-shell species HNO plays a role in the conversion of reactive nitrogen, particularly for non-hydrocarbon fuels such as CO and H_2, by reducing NO due to an important route from NO to nitrogen through the amine radical pool [107]. As mentioned above, NO can promote fuel oxidation by converting stable $H\dot{O}_2$ radicals into active $\dot{O}H$ radicals *via* R–7. However, NO can also inhibit fuel oxidation through a catalyzing recombination process, followed by the removal of free radicals *via* the following reaction sequence:

$$NO + \dot{H} \,(+M) = HNO \,(+M) \quad \textcolor{red}{R25}$$

$$HNO + \dot{H} = NO + H_2 \quad \textcolor{red}{R26}$$

$$HNO + \ddot{O} = NO + \dot{O}H \quad \textcolor{red}{R27}$$

$$HNO + \dot{O}H = NO + H_2O \quad \textcolor{red}{R28}$$

$$HNO + NO_2 = NO + HONO \quad \textcolor{red}{R29}$$

Overall, the HPL of R25 recommended by Tsang and Herron [107] is widely accepted and used in most combustion mechanisms. However, a large uncertainty remains in the LPL of R25. For instance, Allen et al. [108] estimated the LPL against their turbulent flow reactor experiments. It is three times lower than the recommendation of Tsang and Herron [38] but is in satisfactory agreement with the Glarborg et al. [107] experiments. Riley et al. [109] recently measured the rate constant of R25 with Ar as the collider. Their result generally confirmed the values derived by Allen et al. and Glarborg et al. We have therefore selected the recommendation of Tsang and Herron for the HPL, and the values of Glarborg et al. and Allen et al. for the LPL. The third body collision efficiencies are taken from Konnov's [13] estimation.

Soto et al. [110] calculated the potential energy surface (PES) for H-atom abstraction *via* reaction R26 at two levels of theory, multi-configurational self-consistent-field and configuration interaction involving all single and double substitutions. At 1000 K their calculated rate constant is 4.3 times faster than that recommended by Tsang and Herron [38]. Recently, Nguyen et al. [111] re-calculated the rate constants for abstraction not only by $\dot{H}$ atoms but also by $\ddot{O}$ atoms at temperatures of 200 – 2500 K. Their results confirmed Soto et al calculation but they are considerably higher than the value recommended by Tsang and Herron. Compared to R26, H-atom abstraction *via* reaction R28 is a barrier-less reaction. Similarly, the rate constants determined by Nguyen et al. [111] are much lower than the recommendation of Tsang and Herron, and are within a factor of 1.6 of those calculated by Soto et al. [112]. We have used the values of Soto et al. to describe R26 and R28, and this is consistent with the literature models [9, 10, 13, 15, 39]. Moreover, the indirect measurement of Inomate et al. [113] is selected for R27. Similar to the study by Chain et al. [40], Mebel et al. [114] found that despite the fact that *trans*-HONO is the more stable species, the dominant products are *cis*-HONO + NO *via* R29 due to the lower energy barrier. In *this work*, we have adopted the expression calculated by Mebel et al. for R29. It is worth noting that the chemistry of HNO still has large uncertainties, as stated in the work of Faßheber et al. [115]. Direct measurements and theoretical calculation for R25–29 are still poorly investigated, particularly at high temperatures. Experimental/theoretical determinations of the temperature- and/or pressure-dependency of reactions involving HNO would be valuable to the combustion community.

2.2.5.2 HON scheme

In addition to R25, $\dot{H}$ atoms can also be eliminated *via* the reaction:

$$\text{NO} + \dot{\text{H}} \ (+\text{M}) = \text{HON} \ (+\text{M}) \quad \text{R30}$$
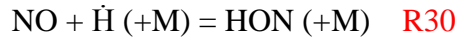
Once HON is formed *via* R30 it can compete with HNO for free radicals *via* the following reactions:

$$\text{HON} + \dot{\text{H}} = \text{HNO} + \dot{\text{H}} \quad \text{R31}$$

$$\text{HON} + \dot{\text{H}} = \text{NH} + \dot{\text{OH}} \quad \text{R32}$$

$$\text{HON} + \ddot{\text{O}} = \text{NO} + \dot{\text{OH}} \quad \text{R33}$$

$$\text{HON} + \text{O}_2 = \text{NO}_2 + \dot{\text{OH}} \quad \text{R34}$$

Amongst these, the branching ratio between R31 and R32 appears to be particularly important for NO formation. Fig. 5 illustrates the effect of including HON chemistry in the simulations, and particularly R32, on NO formation at a typical JSR conditions. It can be seen that the prediction with HON chemistry presents a lower rate of NO formation at higher temperatures (> 850 K), and is closer to the experimental measurements, Fig. 5(a). It means that HON chemistry overall promotes the conversion of NO. Moreover, a sensitivity analysis of NO formation also reveals the importance of R32. The significant effect of an increase in the rate constant of R32 by a factor of two is shown by the solid black line, exhibiting a 30% lower prediction in NO concentration at 1050 K, Fig. 5(b). Note that HON chemistry only plays an important role at atmospheric pressures and at fuel-rich conditions. However, the effect appears to be negligible at higher pressures because the conversion of NO to NO_2 is primarily governed by R5 and R–7. In *this study*, all of the kinetic parameters for HON related reactions are adopted from the recommendations of Dean and Bozzelli [98]. Unfortunately, no further literature data are currently available and further theoretical and experimental studies on this system are warranted.
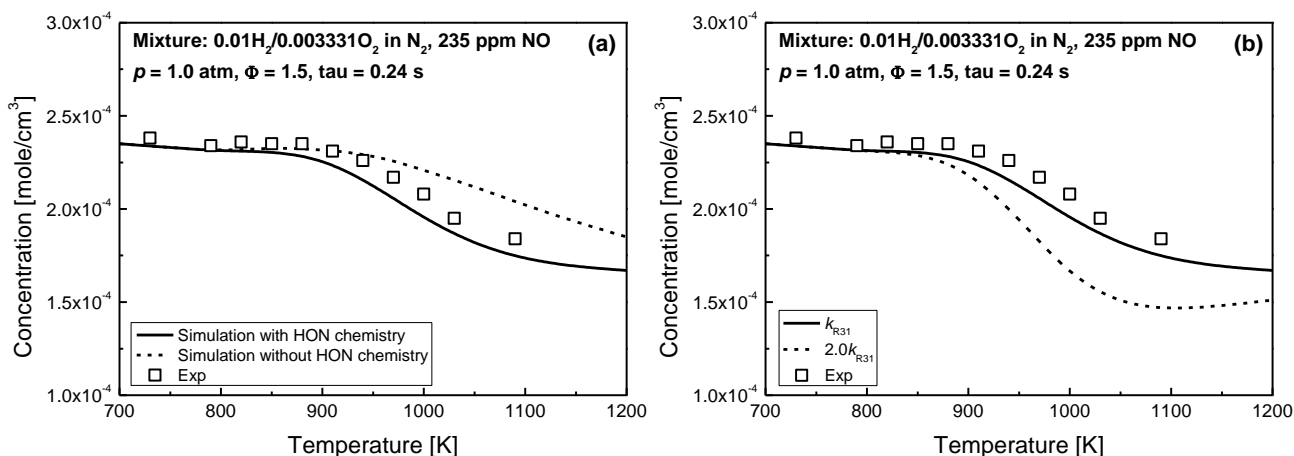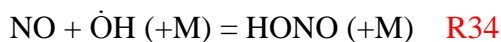
Fig. 5. Effects of HON chemistry and reaction R31 on NO formation in the $H_2/O_2/NO_x$ reaction system at low pressure under fuel-rich condition. (a) Effect of HON chemistry. (b) Effect of rate constant of R32.
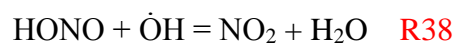
2.2.5.3 HONO/HNO₂ scheme

HONO can be formed by the reaction of HNO with NO_2 *via* R29, while HONO can rapidly

equilibrate with NO and $\dot{O}H$ radicals *via* R34.

$$NO + \dot{O}H\ (+M) = HONO\ (+M) \quad \text{R34}$$

The flux analyses presented in the work of both Mueller et al. [10] and Rasmussen et al. [9] indicate

that, the HONO formed in R29 dissociates directly to participate into the chain propagating sequence

consisting of R25, R29 and R–34, as well as R30 (in our mechanism). Fulle et al. [116] measured the

rate constant at pressures of 1 – 1000 bar and at temperatures of 250 – 400 K. The experimental

measurements are generally in agreement with the LPL recommended by Tsang and Herron [38],

whereas it appears to be over four times higher than that of Tsang and Herron for the HPL. Recently,

Atkinson et al. [117] reviewed the rate constant measurements and derived both the LP and HPLs

which are much closer to the Fulle et al. measurements. On the basis of the more extensive review by

Atkinson et al. in accordance with Fulle et al. measurements, we select the Atkinson et al.

recommendation for R34. Note that the rate constants derived from either Atkinson et al. or Fulle et

al. are only valid in the low temperature range (< 500 K), and thus further experimental/theoretical studies of R34 over a wider range temperature are recommended.

Again, the consumption of HONO mainly undergoes attack of free radicals *via* the following reactions:

$$HONO + \dot{H} = HNO + \dot{O}H \quad \text{R35}$$

$$HONO + H = NO + H_2O \quad \text{R36}$$

$$HONO + \ddot{O} = NO_2 + \dot{O}H \quad \text{R37}$$

$$HONO + \dot{O}H = NO_2 + H_2O \quad \text{R38}$$

$$HONO + NO_2 = HONO_2 + NO \quad \text{R39}$$

$$HONO + HONO = NO_2 + NO + H_2O \quad \text{R40}$$

Hsu et al. [118] theoretically calculated rate constants for the reactions of R35 and R36 using modified G2 and BAC-MP4 methods with TST and RRKM approaches, and the calculated rate constants have been successfully applied to reproduce their subsequent measurements for thermal reduction process of NO_2 by H_2 [88]. This thus gives us a confidence in using the Hsu et al. calculations in our mechanism. In contrast to the reactions R35 and R36, fewer studies of the reaction of HONO with $\ddot{O}$ atoms, R37, have been performed, and Tsang and Herron [38] recommendation is used in our model due to its widely available temperatures. Mueller et al. [10] pointed out that the formation and consumption of HONO is quite sensitive to R38, especially at high-pressure, low temperature conditions. Recently, Xia and Lin [119] performed an *ab initio* calculation of the rate constant for R38 using orbital and variational TST theory. Their results indicated that R38 exhibits a noticeable negative temperature dependence at temperatures below 1000 K. Note that Xia and Lin calculation did not agree with the recommendation of Tsang and

Herron [38], but it was consistently in excellent agreement with Burkholder et al. [120] experimental measurements and Wang et al. [121] theoretical calculations. We therefore use the rate constant from Xia and Lin for R38. Furthermore, Lu et al. [122] carried out an *ab initio* molecular-orbital calculation on R39 in association with TST theory. Here, we re-fit the total rate based on combining the three-parameter fit for *cis*-HONO and *trans*-HONO to assign a rate constant for R39. However, a slightly large uncertainty factor of three to four is present in the rate constant calculation due to the energy barrier uncertainty of $2 - 3$ kcal mol^{-1} resulting from the G2M (RCC, MP2) level of theory used in the determination of the transition state parameters. The bimolecular decomposition of HONO *via* R40 has been calculated by Mebel and Lin [123] with a consistent theory approach of their previous work [122] of R39. We have chosen their calculation in the current model.

As a structural isomer of HONO, the fate of the less stable HNO$_2$ species must also be established. At combustion conditions, two possibilities to form HNO$_2$ proceed through R8 and R9. HNO$_2$ consumption can proceed either *via* isomerization (R41) to form the more stable HONO isomer through inter-conversion of a $\dot{\text{H}}$ atom from N-atom to O-atom or H-atom abstractions by $\ddot{\text{O}}$ atoms *via* R42 and by $\dot{\text{O}}$H radicals *via* R43.

$$\text{HNO}_2 \ (+\text{M}) = \text{HONO} \ (+\text{M}) \quad \text{R41}$$

$$\text{HNO}_2 + \ddot{\text{O}} = \text{NO}_2 + \dot{\text{O}}\text{H} \quad \text{R42}$$

$$\text{HNO}_2 + \dot{\text{O}}\text{H} = \text{NO}_2 + \text{H}_2\text{O} \quad \text{R43}$$

Rasmussen et al. [9] estimated the fall-off behavior for R41 using QRRK analysis based on their PES (47.3 kcal mol^{-1} for HNO$_2$ and 55.3 kcal mol^{-1} for HONO) which is generally consistent with the Takane and Fueno [124] calculations (45.7 kcal mol^{-1} for HNO$_2$ and 56.6 kcal mol^{-1} for HONO) and the determinations of Lu et al. [125] (46.5 kcal mol^{-1} for HNO$_2$ and 55.2 kcal mol^{-1} for HONO).

Note that the LP and HPL expressions for R41 were reported by including a reduction of 17.4 kcal mol^{-1} in the activation energy in light of an Eckart correction [126] for H-atom tunneling. However, in the recent work of Asatryan et al. [127], the heat of formation of HONO (−18.9 kcal mol^{-1}) at 298 K calculated by high level composite methods is 8 kcal mol^{-1} lower than for the HNO$_2$ isomer (−10.9 kcal/mol), while this difference in heat of formation for the isomerization is in excellent agreement with that of Rasmussen et al., and we therefore adopt their rate coefficient to describe R41. Furthermore, Rasmussen et al. calculated the rate constant for reaction R43 at the same level of theory and it is also used in this model. Compared to R41 and R43, R42 is much less important and its rate constant is taken from Dean and Bozzelli [98].
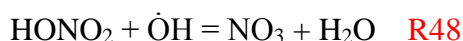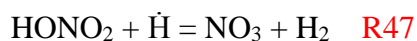
2.2.5.5 HONO$_2$ scheme

The formation of HONO$_2$ through the recombination of NO$_2$ with ȮH radicals, R44, appears to be only important as an ȮH radical-sink at atmospheric pressure. At typical combustion conditions, however, the generated HONO$_2$ is only an intermediate adduct of R−7 and is readily re-dissociation back to the formation of NO$_2$ and ȮH radicals, as discussed by Rasmussen et al. [9].

$$NO_2 + \dot{O}H \, (+M) = HONO_2 \, (+M) \quad \textcolor{red}{R44}$$
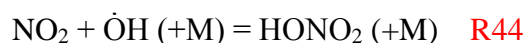
We use the refined fall-off curves reported by Troe [128] as these results are consistent with his previously theoretical work [129] as well as with the experimental measurements [128, 130].

HONO$_2$ is mostly consumed by attack by Ḣ atoms and ȮH radicals *via* the following four reaction channels:

$$HONO_2 + \dot{H} = HONO + \dot{O}H \quad \textcolor{red}{R45}$$

$$HONO_2 + \dot{H} = NO_2 + H_2O \quad \textcolor{red}{R46}$$

$$HONO_2 + \dot{H} = NO_3 + H_2 \quad \textcolor{red}{R47}$$

$$HONO_2 + \dot{O}H = NO_3 + H_2O \quad \textcolor{red}{R48}$$

Here, we have used the recommended rate expressions from Boughton et al. [120] with quantum-mechanical tunneling corrections for the reactions of R45 – R47. By contrast, R48 is more likely critical to combustion of energetic materials related to ammonia. Xia and Lin [131] recently explored the mechanism of R48 *via* an *ab initio* molecular orbital calculations at the G2M(cc3) level of theory. Their calculations reproduce well the experimental observation of a strong negative temperature coefficient behavior [132-135]. In this model, we have chosen the Xia and Lin calculation for R48. Note that the selected value is similar to the measurements of Lamb et al. [136] which have been widely used as a validation target in recent kinetic models [9, 13, 15, 39] and is also consistent with the IUPAC recommendation [117] at 300 K, whereas it is approximately an order of magnitude faster than the Lamb et al. and IUPAC values at 1000 K.

2.2.6 NH$_3$ sub-mechanism

Ammonia (NH$_3$) chemistry partially influences the sub-mechanisms of N/O and H/N/O and further effect the formation of NO$_x$ and thus we have added an NH$_3$ sub-mechanism in our model. The reactions involving NH$_3$ are mostly taken from the recent work of Mathieu and Petersen [137] where the NH$_3$ scheme was modified based on the model proposed by Dagaut et al. [59]. The updated model is capable of predicting the shock tube ignition delay time [137] and species profiles [59] for NH$_3$/O$_2$/Ar mixtures over a wide range of conditions. The sub-schemes of the NNH and NH$_2$OH species recently reported by Klippenstein et al. [39, 73] are adopted to describe thermal DeNO$_x$.

3. Model performance

A great deal of experimental data measured using shock tubes, JSRs, flow reactors and spherical combustion bombs were collected to assess the performance of the mechanism developed in *this study*. In total, over 104 shock tube data sets, 87 JSR data sets, 87 flow reactor data sets and 6 laminar flame speed data sets have been used for the validation and comparison which are included as Supplementary material. The selected data are summarized in Table 1. Furthermore, five recent mechanisms available in the literature, namely the Ahmed_2016 mechanism [15], the Konnov_2009 mechanism [13], the SJK/PG_2015 mechanism [31, 39], the Mével_2009 mechanism [19] and the Dagaut_2008 mechanism [59] were also used to compared with the experimental targets as well as the model developed here.

Table 1. Range of Experimental devices and conditions used for mechanism improvement and validation

Experimental device	Measured properties	Experimental conditions	Reference
Shock tube	Species profiles (2 data sets)	2.2 atm, 2150 – 2800 K, $\varphi = 0.167 – 3.0$ for $H_2/O_2/N_2$ mixtures	Bowman [17] 1971
Shock tube	Species profiles (29 data sets)	58 – 347 kPa, 1490 – 2490 K for N_2O/Ar mixtures	Javoy et al. [20] 2009
Shock tube	Species profiles (4 data sets)	8.0 – 11.5 atm, 1800 – 2700 K for $H_2/N_2O/Ar$ mixtures	Zuev and Starikovskii [21] 1991
Shock tube	Ignition delay times (15 data sets)	1.5 – 30 atm, 1038 – 1744 K, $\varphi = 0.3 – 1.0$ for $H_2/O_2/NO_2/Ar$ mixtures	Mathieu et al. [8] 2013
Shock tube	Ignition delay times (12 data sets)	1.6 – 32 atm, 940 – 1675 K, $\varphi = 0.5$ for $H_2/O_2/N_2O/Ar$ mixtures	Mathieu et al. [18] 2012
Shock tube	Ignition delay times (3 data sets)	1.8 – 32 atm, 993 – 1975 K, $\varphi = 0.5$ for $H_2/CO/O_2/NH_3/Ar$ mixtures	Mathieu et al. [16] 2013
Shock tube	Ignition delay times (2 data sets)	0.14 – 0.47 atm, 1007 – 1574 K For $H_2/N_2O/Ar$ and $H_2/O_2/N_2O/Ar$ mixtures	Kosarev et al. [22] 2007
Shock tube	Ignition delay times (9 data sets)	300 kPa, 1300 – 2000 K, $\varphi = 0.5 – 2.0$ for $H_2/N_2O/Ar$ mixtures	Mével et al. [19] 2009
Shock tube	Ignition delay times and species	1.29 – 1.91 atm, 1700 – 2600 K, $\varphi = 0.36 –$	Henrici and Bauer

	profiles (7 data sets)	1.0 for H$_2$/N$_2$O/Ar mixtures	[23] 1969
Shock tube	Ignition delay times (3 data sets)	2.0 atm, 1400 – 2000 K, $\varphi = 0.5 – 2.0$ H$_2$/N$_2$O/Ar mixtures	Hidaka et al. [24] 1985
Shock tube	Ignition delay times (2 data sets)	1.5 atm, 1919 – 2781 K, $\varphi = 3.3 – 5.0$ for H$_2$/N$_2$O/Ar mixtures	Pamidimukkala and Skinner [25] 1982
Shock tube	Ignition delay times (2 data sets)	1.4 – 10.4 atm, 1654 – 2221 K for H$_2$/CO /N$_2$O/Ar mixture	Kopp et a. [27] 2012
Shock tube	Ignition delay times (2 data sets)	3.0 – 12 atm, 1436 – 2287 K for N$_2$O/Ar mixture	Borisov et al. [138] 1972
Shock tube	Ignition delay times (12 data sets)	1.4 – 30 atm, 1560 – 2455 K, $\varphi = 0.5 – 2.0$ for NH$_3$/O$_2$/Ar mixtures	Mathieu and Petersen [137]
JSR	Species profiles (78 data sets)	1.0 – 10 atm, 700 – 1150 K, $\varphi = 0.1 – 2.5$ for H$_2$/O$_2$/NO$_x$/N$_2$ mixtures	Dayma and Dagaut [28] 2006
JSR	Species profiles (9 data sets)	1.0 atm, 800 – 1400 K, $\varphi = 0.1 – 2.0$ for H$_2$/CO/O$_2$/NO$_x$/N$_2$ mixtures	Dagaut et al. [30] 2003
Flow reactor	Species profiles (4 data sets)	50 atm, 702 – 900 K, $\varphi = 0.0009 – 12$ for H$_2$/O$_2$/N$_2$ mixtures	Hashemi et al. [55] 2015
Flow reactor	Thermal NO (4 data sets)	1.0 atm, 1700 – 1800 K, 0.45 – 20.% O$_2$ for O$_2$/N$_2$ mixtures	Abian et al. [31] 2015
Flow reactor	Species profiles (15 data sets)	20 – 100 atm, 600 – 900 K, $\varphi = 0.064$ for CO/H$_2$/O$_2$/NO$_x$ mixture	Rasmussen et al. [9] 2008
Flow reactor	Species profiles (41 data sets)	0.5 – 14 atm, 750 – 1100 K, $\varphi = 0.25 – 1.0$ for H$_2$/O$_2$/NO$_x$ and CO/H$_2$O/O$_2$/NO$_x$ mixtures	Mueller et al. [10] 1999
Flow reactor	Species profiles (23 data sets)	1.05 atm, 800 – 1400 K for NO/NO$_2$/CO/H$_2$O/N$_2$ mixtures	Glarborg et al. [32] 1995
Spherical combustion bomb	Laminar flame speeds (1 data set)	1.0 atm, 300 K, $\varphi = 0.15 – 1.8$ for H$_2$/N$_2$O/Ar mixtures	Mével et al. [33] 2009
Spherical combustion bomb	Laminar flame speeds (5 data set)	0.2 – 0.8 atm, 298 K, $\varphi = 0.15 – 1.0$, 0 – 55% N$_2$ for H$_2$/N$_2$O/N$_2$ mixtures	Bane et al. [34] 2011

3.1. Zeldovich NO formation

Bowman [17] conducted an investigation of thermal NO formation for H$_2$/O$_2$/N$_2$ combustion at an average pressure of 2.2 atm over temperature range 2150 – 2800 K using a shock tube and he provided the concentration of NO in two vibrational states ($v = 1$ and $v = 2$) corresponding to the

absorption of incident radiation by both of the molecular bands ($\gamma(0, 1)$ and $\gamma(0, 2)$). Concentration profiles of $\dot{O}H$ radicals, NO ($v = 1$) and H_2O were measured and were simulated using the current model. The results are in very good agreement with Bowman's measurements within his experimental uncertainty, Fig. 6(a).
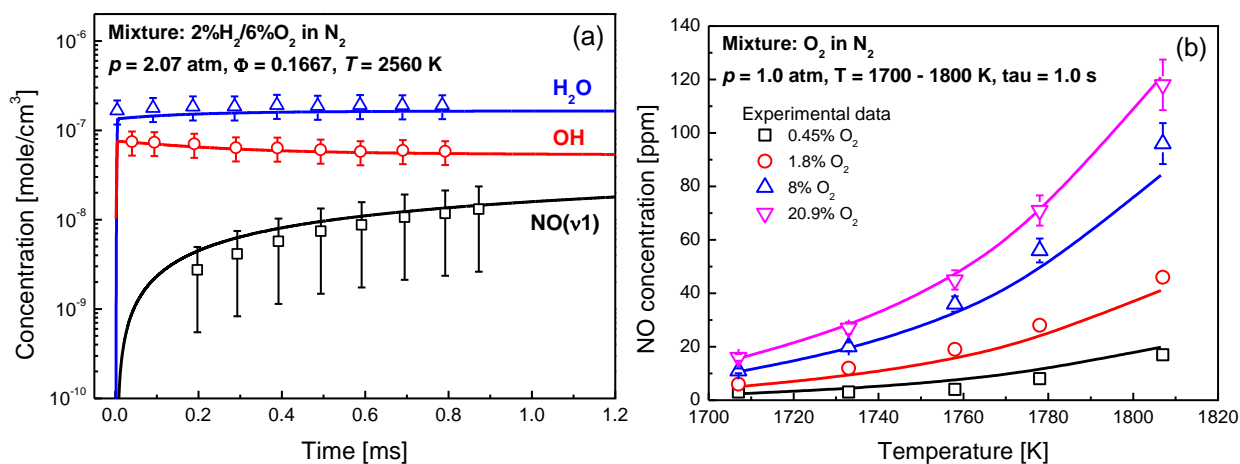

Fig. 6. Comparison of experiments and model predictions for Zeldovich NO formationin in O_2/N_2 system with different O_2 concentrations. Symbols represent experimental measurements; lines denote model simulation with the current mechanism. (a) Shock tube data of Bowman [17]. (b) Flow reactor data of Abian et al. [31].

In addition, Abian et al. [31] recently measured thermal NO formation in N_2/O_2 oxidation using a flow reactor with various O_2 concentrations (0.45% − 20.9%) at temperatures in the range 1700 − 1800 K and at atmospheric pressure. To confirm the validity of the Zeldovich mechanism in our model the data reported by Abian are also used to validate model predictions. Likewise, the model gives excellent agreement with the experimental measurements, Fig. 6(b). More validations are provided in Figs. S2 and S3.

3.2. Ignition delay times

Shock tube measurements involving global combustion targets of ignition delay times and pyrolysis of nitrogenous species are primarily used to examine the validity of the current mechanism.

These experiments were carried out over a wide range of pressure (0.14 – 33 atm), temperature (940 – 2600 K), equivalence ratio (0.3 – 5.0) and NO_x concentration (100 ppm – 10%) for different reaction systems such as pure N_2O, H_2/N_2O, $H_2/NO_x/O_2$, and $H_2/CO/N_2O$ system. Complete validations are presented in Figs. S4–S17, and only typical cases will be discussed below.

3.2.1 Model performance

3.2.1.1 N_2O pyrolysis and self-oxidation

When a fuel and molecular oxygen are absent in a reaction system, the N_2O chemistry only involves its decomposition mechanism (i.e. R11, R15, R16 and R19) and the Zeldovich mechanism. Javoy et al. [20] explored the decomposition of N_2O by experimentally monitoring the formation of Ö atoms behind reflected shock waves at pressures of 0.58 – 3.47 atm in the temperature range 1490 – 2490 K. Borisov and Skachkov [26] also used a shock tube to investigate the spontaneous ignition behavior of N_2O/Ar mixtures at pressures of 2.5 – 14 atm in the temperature range 1351 – 2326 K. The data measured in both of these studies are compared to the current model predictions, Fig. 7. It can be seen that the current model reproduces well the temperature dependence of Ö atom formation as well as the pressure dependence of the self-ignition delay times of N_2O.
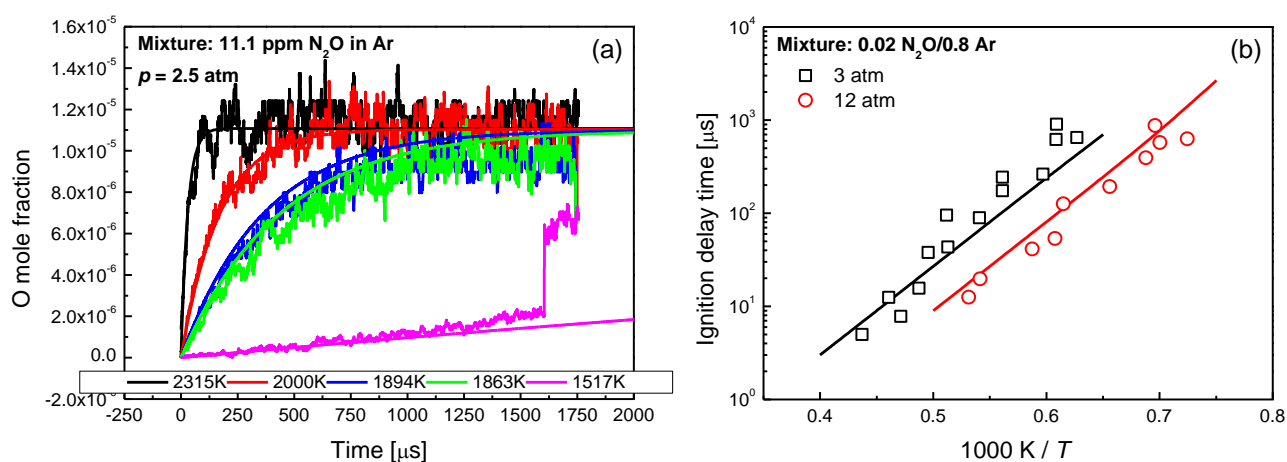

Fig. 7. Comparison of experiments and model predictions for the pyrolysis and oxidation of N_2O/Ar mixtures at pressures of 2.5 – 12 atm. Symbols represent experimental measurements; lines denote

model simulations with the current mechanism. (a) Shock tube absorption profiles of Ö atoms taken from Javoy et al. [20]. (b) Shock tube ignition delay times taken from Borisov and Skachkov [26].

3.1.2.3 $H_2/NO_x/O_2$ system

The $H_2/NO_2/O_2$ and $H_2/N_2O/O_2$ systems are considered as the targets to explore the interaction of hydrogen and NO_x in the presence of O_2. Mathieu et al. [8, 18] conducted a series of shock tube investigations on the effect of NO_2 and N_2O addition on the ignition of H_2/O_2 mixtures at various pressures (1.5 – 33 atm), equivalence ratios (0.5 – 2.0) and NO_x concentrations (100 – 1600 ppm for NO_2 addition and 100 – 3200 ppm for N_2O addition). The ignition delay time data of Mathieu et al. are therefore used to compare to the current model predictions. Results of the model simulations are in excellent agreement with the experimental data, Fig. 8. For the addition of low concentrations of NO_2, the pressure-dependence of the ignition delay times is essentially consistent with that for pure hydrogen. This means that NO_2 only has a limited perturbation effect on the kinetics of hydrogen oxidation, Fig. 8(a).
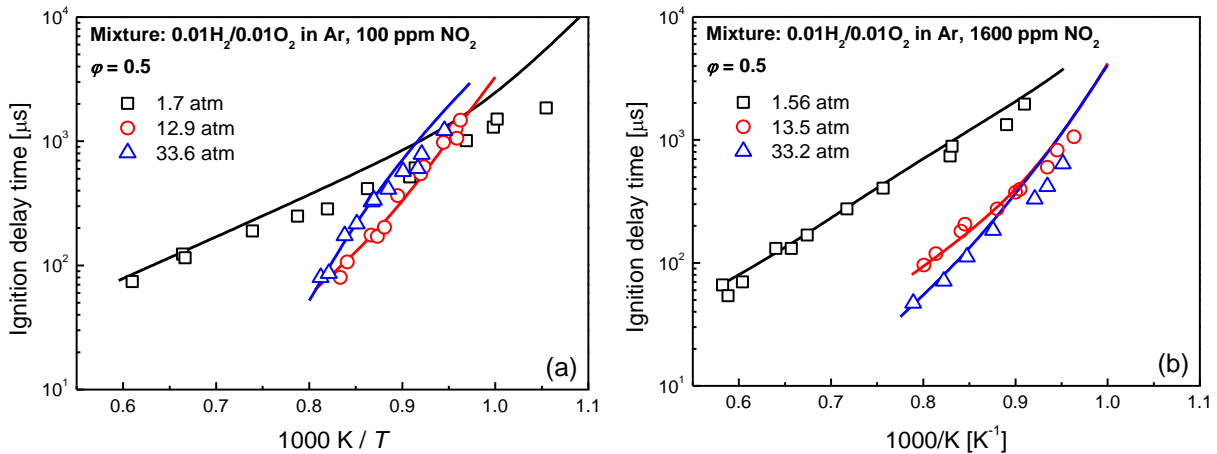

Fig. 8. Comparison of experiments and model predictions for ignition delay times of $H_2/O_2/NO_2/Ar$ mixtures. Symbols represent experimental measurements taken from Mathieu et al. [8]; lines denote model simulations with the current mechanism. (a) Effect of pressure at low concentration of NO_2. (b) Effect of pressure at high concentration of NO_2.

For high levels of NO_2 addition, NO_2 has a strong pressure-dependence only at lower pressures (from 1.5 to 13.5 atm), whereas it was reported that there appeared to be a weak pressure dependence at higher pressures (from 13.5 to 33.2 atm), Fig. 8(b). As discussed by Mathieu et al. [8], for high levels of NO_2 in the hydrogen system, reactions governing ignition change from a chain branching reaction ($\dot{H} + O_2 = \ddot{O} + \dot{O}H$ (R_{H1})) to a chain propagating reaction ($H_2 + \dot{O}H = \dot{H} + H_2O$ (R_{H2})) due to the additional generation of $\dot{O}H$ radicals, which results in an equilibrium of the radical-pool concentration.
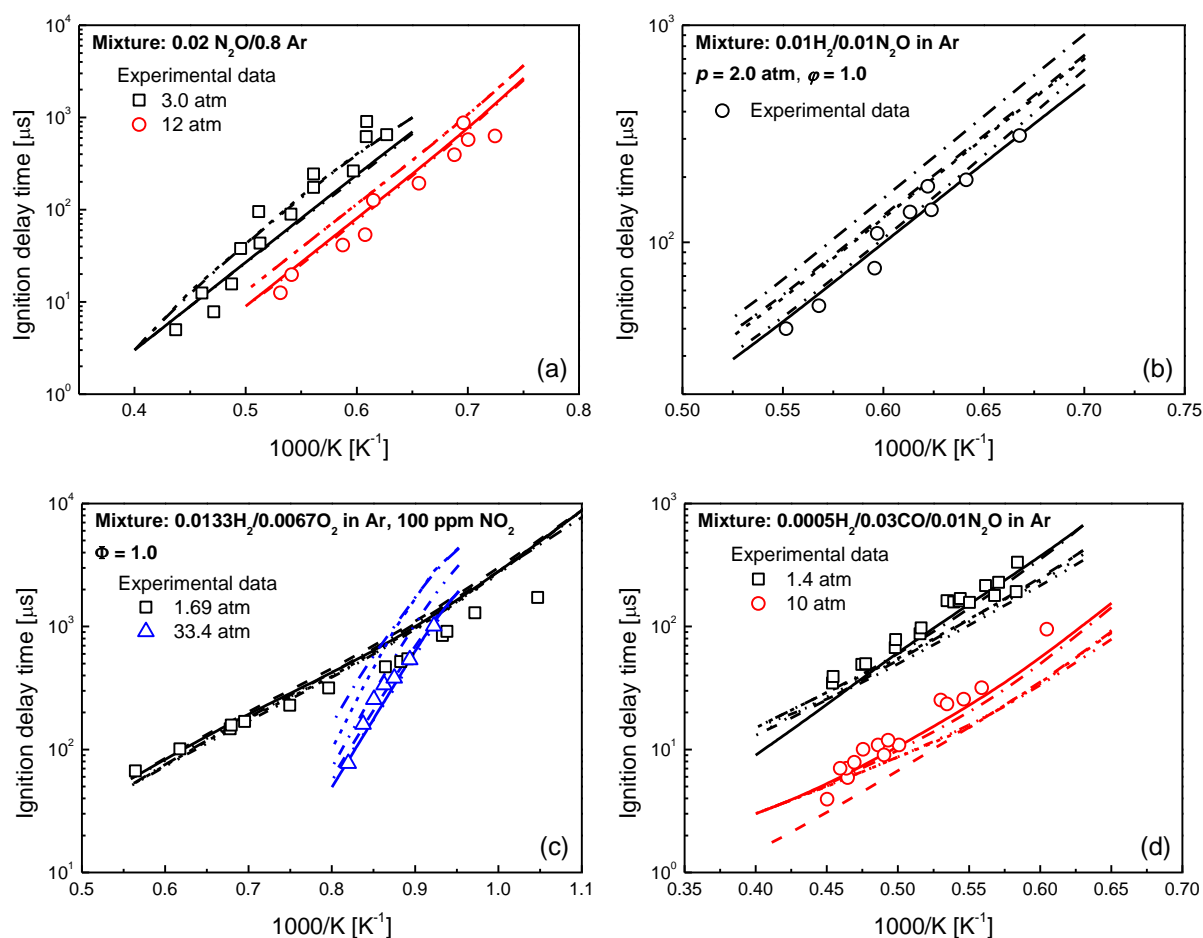
Fig. 9. Current model and selected literature model predictions compared to literature data. Symbols represent experimental measurements; lines denote model simulations with the current model (solid line), Ahmed_2016 [15] (dash line), Konnov_2009 [13] (dot line), SJK/PG_2015 [31, 39] (dash dot line), Mével_2009 [19] (dash dot dot line) and Dagaut_2008 [59] (short dash line). (a) N_2O self-oxidation without fuel and O_2 [26]. (b) H_2/N_2O oxidation without O_2 [24]. (c) $H_2/NO_2/O_2$ oxidation [8]. (d) $H_2/CO/N_2O$ oxidation [27].

3.2.2 Comparison with literature models

Fig. 9 shows a comparison of the current model prediction with the performances of five literature models against the experimental measurements for the five typical systems mentioned above. Overall, the different models predict the ignition delay times reasonable well and this conclusion is in consensus with Ahmed et al. [15]. The SJK/PG_2015 mechanism over-predicts the reactivity of the $H_2/N_2O/Ar$ system (Fig. 9(b)) at low pressures while the SJK/PG_2015 and Dagaut_2008 mechanisms over-predict the reactivity of the $H_2/O_2/NO_x/Ar$ system at high pressures (Fig. 9(c)). It should be noted that the different models present different predictions of the experimentally observed global activation energy for the $H_2/CO/N_2O/Ar$ system at 10.4 atm. The SJK/PG_2015 model and our mechanism are in good agreement with the experimental data whereas the other five models give slightly lower activation energy value, Fig. 9(d). The reason for the difference may be a combination of a) the different base chemistry (H_2 and CO), b) the different sub-mechanisms for N_2O and NO_2 chemistry and c) the different sources of thermochemistry used.

3.3. Flow reactor species versus time data

In an attempt to further illustrate the model performance, the evolution profiles of major species versus reaction time and/or temperature measured in FRs have been simulated using the current model. These flow reactor experiments were performed over a wide range of pressure ($0.5 - 100$ atm), temperature ($600 - 1800$ K), equivalence ratio ($0.0009 - 12$) and NO_x concentration ($12 - 10000$ ppm) for different reaction systems including $H_2/NO_x/O_2$, $CO/H_2O/NO_x/O_2$ and $H_2/CO/H_2O/NO_x/O_2$. Complete validations are provided in Figs. S18–S20, and only representative cases are selected for the discussion in the following section.

3.3.1 Model performance

3.3.1.1 $H_2/NO_x/O_2$ system

Fig. 10 depicts detailed comparisons of model predictions of species profile data [10] as a function of time taken over a series of experimental conditions where the pressure was varied from 1.0 to 10 atm. It indicates that increasing the pressure inhibits H_2 consumption and promotes the NO to NO_2 inter-conversion. The model accurately captures the pressure-dependent behavior throughout the entire reaction time scale. Note that the effect of pressure appears to be more noticeable at higher pressures due to the fact that the third-body recombination reaction $\dot{H} + O_2 (+M) = H\dot{O}_2 (+M)$ (R_{H3}) dominates the reactivity at elevated pressures and at intermediate temperatures, namely 806 K in *this study*. The abundant $H\dot{O}_2$ radicals preferentially react with NO to form NO_2 *via* R–7.
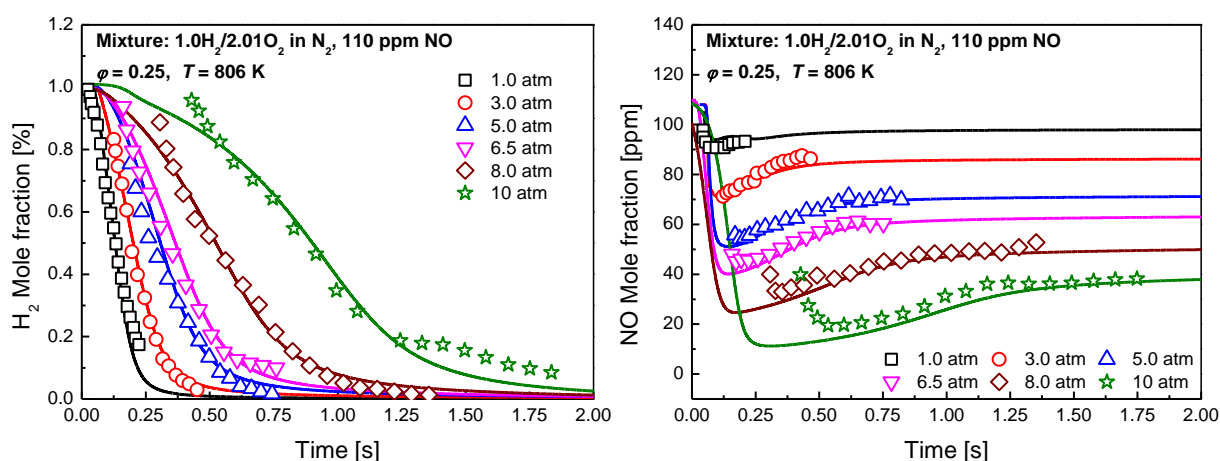

Fig. 10. Comparison of experiments and model predictions for the species profiles in $H_2/O_2/NO/N_2$ mixture at 806 K and elevated pressures in a flow reactor [10]. Symbols represent experimental measurements; lines denote model simulations with the current mechanisms.

3.3.1.3 $H_2/CO/H_2O/NO_x/O_2$ system

For the $H_2/CO/H_2O/NO_x/O_2$ system model predictions are compared with the high pressure FR species profiles of Rasmussen et al. [9] at pressures of 20 − 100 atm, Fig. 11. Again, the model thoroughly reproduces the pressure dependence of the CO to CO_2 conversion as well as the evolution

of the NO_x species. In general, increasing the pressure reduces the initial temperature of the CO to CO_2 conversion process. The effect of pressure on the initial temperature of CO consumption reduces with increasing pressure. This is as expected as indicated by Rasmussen et al. [9] and Ahmed et al. [15]. Note that the results simulated with the current model are quite similar to the numerical values of Rasmussen et al, meaning the current model are largely consistent with Rasmussen et al. with respect to considering real temperature profiles.
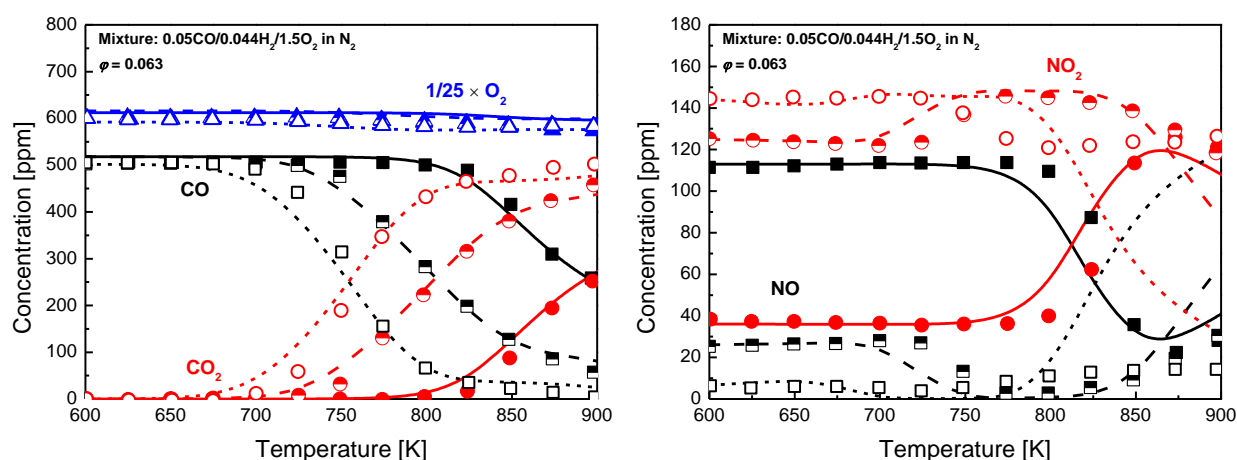

Fig. 11. Comparison of experiments and model predictions for the species profiles in $CO/H_2/NO_x/N_2$ mixture at 100 atm over 600 – 900 K in a flow reactor [9]. Symbols represent experimental measurements (solid: 20 atm, half-solid: 50 atm, open: 100 atm); lines denote model simulations with the current mechanism (solid line: 20 atm, dash line: 50 atm, short dash line: 100 atm).

3.3.2 Comparison with literature models

Unlike the comparison of the model performance in predicting ignition delay times, the current model is considerably different to other literature models in simulating either the $H_2/NO_x/O_2$ system or the $CO/H_2O/O_2$ system. Fig. 12 shows detailed comparisons of the model performance at 10 atm. For the $H_2/NO_x/O_2$ system, Fig. 12(a), both the SJK/PG_2015 and Mével_2009 mechanisms over-predict the consumption of hydrogen, especially at intermediate and late reaction times. As a result, the two models present unreasonable predictions of NO to NO_2 conversion, particularly the SJK/PG_2015 mechanism. Note that the predictions by the Ahmed_2016 mechanism are not

presented at this condition due to convergence issues. However, for the $CO/H_2O/O_2$ system, all of the models generally agree in the prediction of NO formation but they significantly diverge in predicting CO oxidation. Specifically, the Mével_2009 mechanism predicts the slowest consumption of CO whereas the SJK/PG_2015 mechanism presents the fastest consumption. The Ahmed_2016 and Konnov_2009 mechanisms also predict a slightly fast consumption of CO.
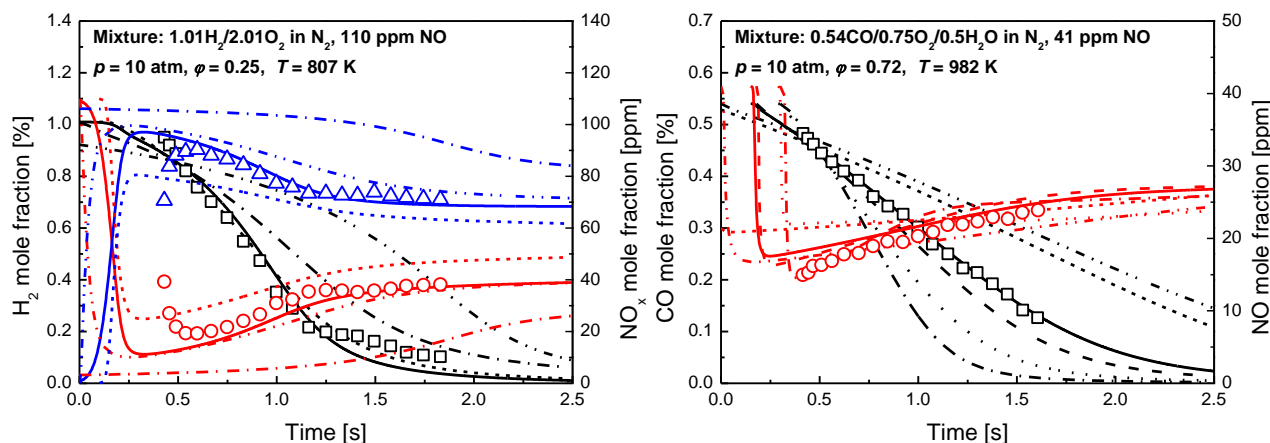

Fig. 12. Current model and selected literature model predictions compared to literature data. Symbols represent experimental measurements [10]; lines denote model simulations with current model (solid line), Ahmed_2016 [15] (dash line), Konnov_2009 [13] (dot line), SJK/PG_2015 [31, 39] (dash dot line), Mével_2009 [19] (dash dot dot line) and Dagaut_2008 [59] (short dash line).

3.4. Jet-stirred reactor species versus temperature profiles

JSR species versus temperature data are used to test the ability of the proposed model by comparing its predictions to major species concentration profiles measured by Dagaut et al. [28, 30]. These JSR experiments were performed over a wide range of pressures (1.0 – 10 atm), temperatures (700 – 1400 K), equivalence ratios (0.1 – 2.5) and NO_x concentrations (70 – 1000 ppm) for different reaction systems including $H_2/NO/O_2$, $H_2/NO_2/O_2$ and $H_2/CO/NO_x/O_2$. All of the data are valuable to provide further insight into the kinetic mechanisms including NO_x formation, NO to NO_2 inter-conversion and the kinetics of interaction of NO_x species with fuel. Complete validations are

available in Figs. S21 and S22. Likewise, we only chose several illustrative cases herein to discuss in the following section.

3.4.1 Model performance

Fig. 13 shows the detailed comparisons of experimental and model predicted species versus temperature profiles for the H_2/O_2 system in the presence of 220 ppm NO at $p = 10$ atm and $\varphi = 0.5$. It is clear that the conversion rate of NO to NO_2 first promotes and then inhibits reactivity with increasing temperature, with the reactivity reaching a peak value at approximately 800 K. The transformation in the conversion rate of NO to NO_2 can be kinetically interpreted by considering the concentration of $H\dot{O}_2$ radicals generated at different temperatures. At lower temperatures (< 800 K), $H\dot{O}_2$ radicals are formed *via* R_{H3}, which promotes the conversion of NO into NO_2. However, as the temperature increases R_{H3} is inferior in competition with R_{H1} resulting in a lower concentration of $H\dot{O}_2$ radicals and low rate of R–7. Meanwhile, additional $\dot{H}$ atoms yielded by reaction sequence R_{H1} and R_{H2} accelerates the rate of R5 leading to the conversion of NO_2 back to NO. As expected, the current model accurately captures the NO to NO_2 inter-conversion as well as H_2 to H_2O conversion.
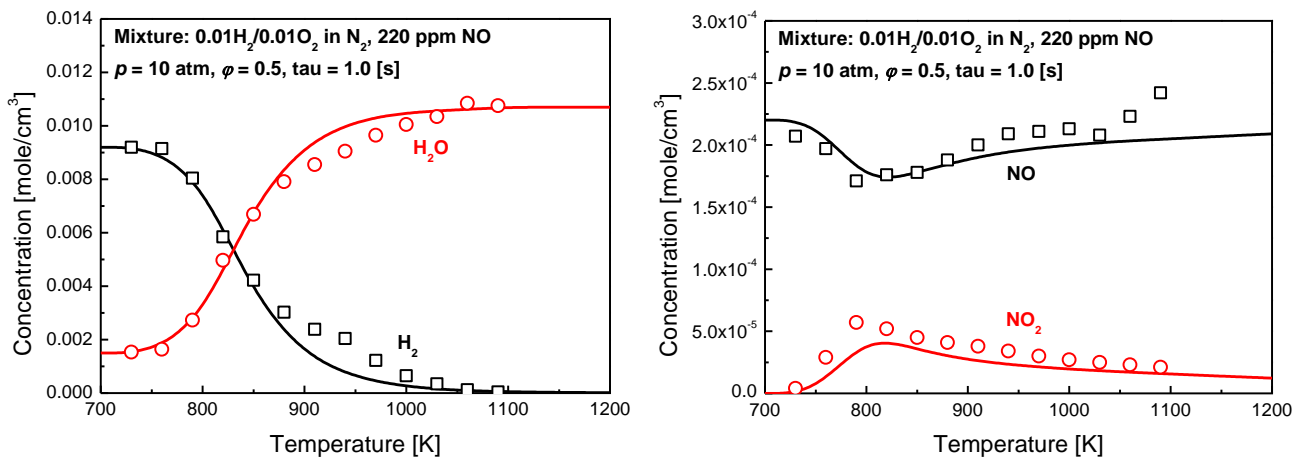

Fig. 13. Comparison of experiments and model predictions for the species profiles in $H_2/O_2/NO/N_2$ system at 1.0 and 10 atm over 700 – 1100 K in a jet-stirred reactor [28]. Symbols represent; lines denote model simulations with the current mechanism.

3.4.2 Comparison with literature models

Here, only two JSR conditions ($p = 1.0$ atm, $\varphi = 2.0$ for the $H_2/O_2/NO$ system and $p = 1.0$ atm, $\varphi = 1.5$ for the $H_2/O_2/NO_2$ system) reported by Dayma and Dagaut [28] are taken as representative cases to test the performance of our proposed model and others in the literature, Fig. 14.

For fuel oxidation, all of the models are in good agreements with the experimental measurements for the addition of both NO and NO_2 except the Konnov_2009 mechanism which shows an under-prediction in the consumptions of reactants resulting in an over-prediction in the formation of H_2O in the $H_2/O_2/NO$ system but the model is in reasonable agreement for the $H_2/O_2/NO_2$ system.
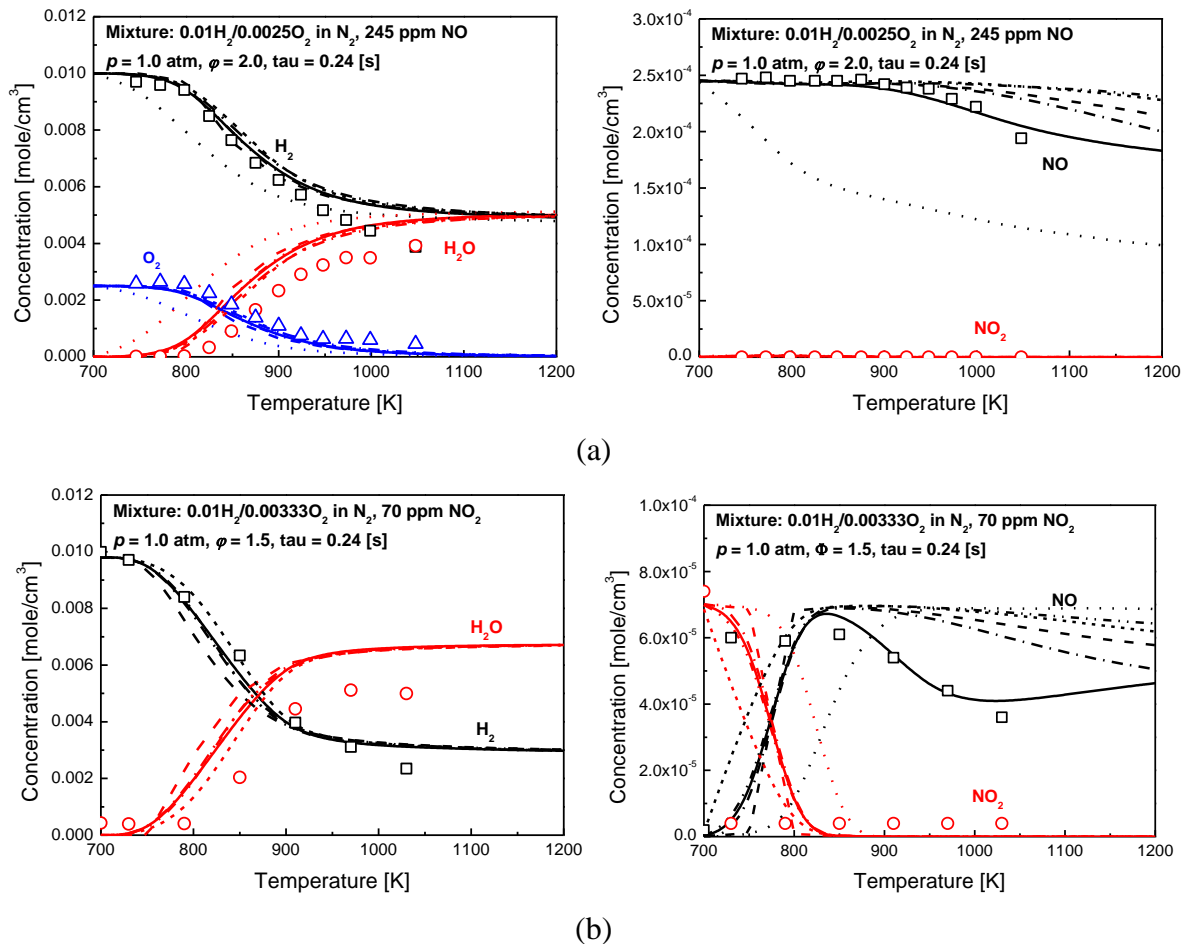
(a)

(b)

Fig. 14. Current model and selected literature model predictions compared to literature data. Symbols represent experimental measurements [28]; lines denote model simulations with the current model (solid line), Ahmed_2016 [15] (dash line), Konnov_2009 [13] (dot line), SJK/PG _2015 [31, 39] (dash dot line), Mével_2009 [19] (dash dot dot line) and Dagaut_2008 [59] (short dash line). (a) H_2/O_2 oxidation under NO perturbation. (b) H_2/O_2 oxidation under NO_2 perturbation.

For the NO to NO_2 conversion process however, noticeable discrepancies in the model simulations can be clearly observed in either the $H_2/O_2/NO$ or the $H_2/O_2/NO_2$ systems. All of the literature models do not predict the decline in the NO concentration at higher temperatures— > 950 K for the $H_2/O_2/NO$ system and > 850 K for the $H_2/O_2/NO_2$ system. Dayma and Dagaut [28] attempted to modify their model's shortcoming by modifying the rate constant of the reactions HNO + H_2 = NH + H_2O and NH + NO = N_2 + $\dot{O}H$, but this change does not appear to be a satisfactory explanation/improvement as the modified model results in poorer predictions of the experiments at high pressures. They thus suggested that more kinetic analysis was needed to clarify this issue. In the current model, we have added the new reaction scheme for HON oxidation as discussed in Section 2.1.4.2, and identified its importance in predicting NO formation/consumption at low pressures. Clearly, the addition of HON chemistry greatly improves the NO conversion kinetics at low pressures yet maintains the model's good predictability at high pressures.

3.5. Spherical flame speeds

Finally, spherical flame data are used to test the fidelity of the proposed model by comparing its predictions to laminar flame speeds measured by Mével et al. [33] and Bane et al. [34]. These experiments were performed over a range of pressures (0.2 – 1.0 atm), equivalence ratios (0.15 – 1.8) and dilutions (0 – 55% for N_2 and 60% for Ar). All of the data are helpful in testing the high temperature chemistry of the H_2/N_2O system. More validations are presented in Figs. S23 and S24.

3.5.1 Model performance

Fig. 15 shows an example case of model predictions of measured laminar flame speed data for two different systems. For the case of the H_2/N_2O system diluted in Ar, the proposed model

generally agrees with the experimental data over the range of equivalence ratios available, Fig. 15(a).

It slightly under-estimates the flame speeds on the fuel-lean side but it in better agreement on the

fuel-rich side. Moreover, our current model is in excellent agreement with the data taken in the

undiluted H_2/N_2O system, Fig. 15(b). The comparative results suggests that the rate constants of the

most important reactions R12 ($N_2O + \dot{H} = N_2 + \dot{O}H$) and R13 ($N_2O + \dot{H} = NH + NO$) in the flame

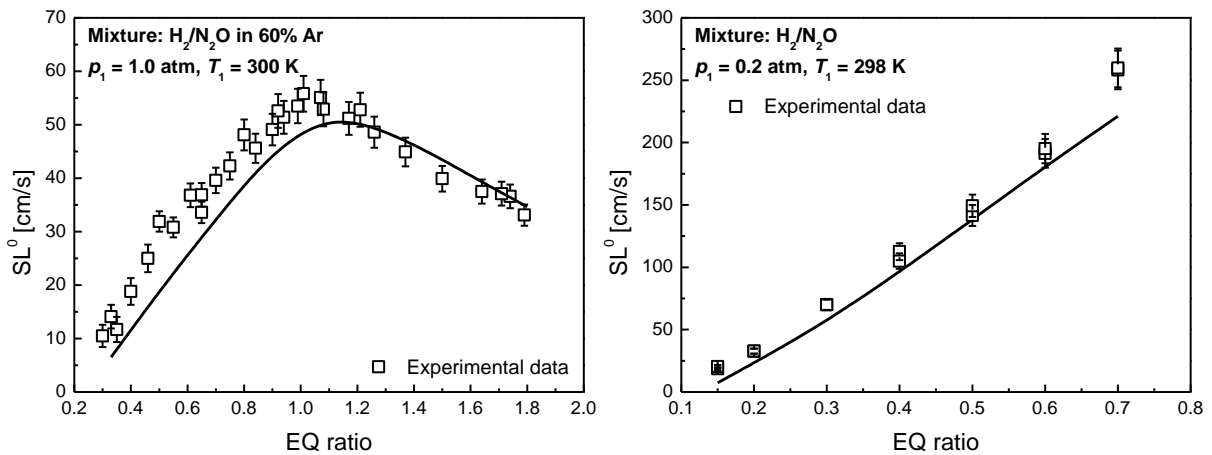conditions highlighted by Mével et al. [33] are reliable in our proposed mechanism.

Fig. 15. Comparison of experiments and model predictions for the laminar flame speeds in H_2/N_2O/dilution system; lines denote model simulation with the current mechanism. Symbols represent experimental measurements for (a) H_2/N_2O diluted by 60% Ar at 1.0 atm and 300 K taken from Mével et al. [33] and for (b) H_2/N_2O undiluted at 0.2 atm and 298 K taken from Bane et al. [34].

3.5.2 Comparison with literature models

The conditions associated with the experiments presented in Fig. 15(a) have been selected as a

representative case to compare the ability of literature models to predict flame speeds. Detailed
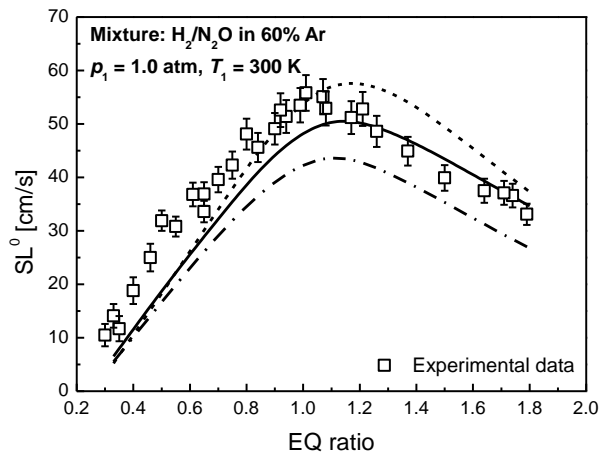
comparisons are provided in Fig. 16.

Fig. 16. Comparison between current model and selected models against literature data. Symbols represent experimental measurements; lines denote model simulations with the current model (solid line), SJK/PG_2015 [31, 39] (dash dot line), and Dagaut_2008 [59] (short dash line).

The results indicate that all of the models tested here predict well the measured flame speeds but the consensus tends to be worse with increasing equivalence ratios. The SJK/PG_2015 mechanism shows an under-prediction while the Dagaut_2008 mechanism over-predicts the flame speeds at richer conditions. Note that the current mechanism and the SJK/PG_2015 mechanism predict a peak value of flame speed at $\varphi = 1.1$ which is consistent with the experimental observations, whereas the Dagaut_2008 mechanism predicts the peak at $\varphi = 1.2$.

It is noted that, we only added part of error bars to the experimental data due to such the reasons: a) the authors did not pointed out clearly the uncertainty of their data and b) the data can be more clearly depicted and compared with modeling without error bars. Mueller et al. data [10] for example, although they gave the uncertainties of measured species (H_2O: 10%; O_2: 3%; CO: 2%; CO_2, 2%; H_2: 5%; NO: 5% and NO_2: 5%), to better distinguish the comparison of different models and the comparison of experimental data and model predictions, we have chosen not to include error bars for clarity as they are already very busy plots.

4. Mechanism application to gas-turbine relevant condition

To provide more kinetic information for combustor design, we have used the proposed model to simulate the pressure-, temperature- and equivalence ratio-dependence of NO concentration for the selected mixture, 50% H_2/50% CO diluted in air, at practical engine-relevant conditions of pressures in the range $10 - 80$ atm, at temperatures of $750 - 1050$ K and at equivalence ratios of $0.1 - 2.0$. Detailed flux analyses were then carried out to better understand the effect of equivalence ratio on NO formation.

4.1. Effect of engine combustion conditions on NO formation

Fig. 17(a) shows the NO concentration as a function of pressure at $T = 850$ K and at various equivalence ratios. It is clear that NO exhibits a weak pressure-dependence at a given equivalence ratio meaning that the ignition pressure within an operating range of between 10 and 80 bar does not appear to have any effect on the concentration of NO formed. In contrast, the effects of temperature and equivalence ratio are more prominent, especially the latter, Fig. 17(b). For a given equivalence ratio, decreasing the temperature leads to a proportional reduction in NO concentration. At $\varphi = 0.5$ for example, a 10 K decrease in temperature reduces the NO concentration by 10 ppm over the temperature range investigated. For a given temperature however, increasing the equivalence ratio first promotes and then inhibits NO formation. The NO concentration reaches a maximum value at $\varphi \approx 0.75$. On either side of this peak value, either fuel-lean or fuel-rich, there is a dramatic reduction in the observed NO concentration. Compared to controlling the pressure and temperature in the reactor, controlling the equivalence ratio of the reactant mixtures in the reactor appears to be more a promising way to control NO formation.
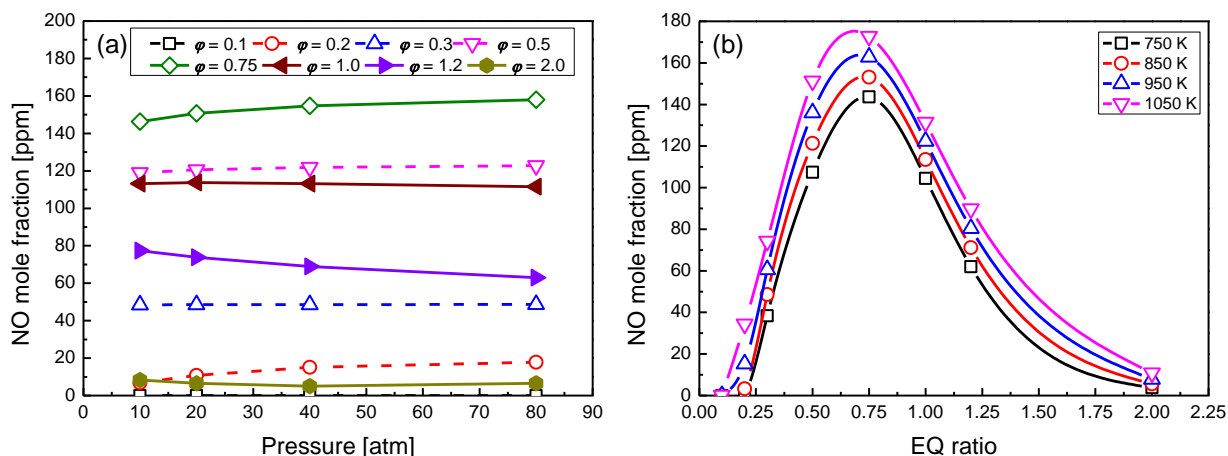
Fig. 17. NO formations calculated using the proposed model for $H_2/CO/O_2/N_2$ system at practical engine conditions. (a) NO formation as a function of pressure at 850 K at various equivalence ratios; (b) NO formation as a function of equivalence ratio at 30 atm and different temperatures.

4.2. Flux analysis

Based on the analysis above, flux analyses were carried out for the same mixtures at $p = 30$ atm and $T = 850$ K to provide an overview of the critical NO formation/consumption pathways at equivalence ratios of 0.3, 0.75 and 2.0, Fig. 18. In the system investigated here, NO is formed from molecular nitrogen. N_2 is therefore selected as the initial reactant to explore the critical reaction pathway governing NO formation/consumption.
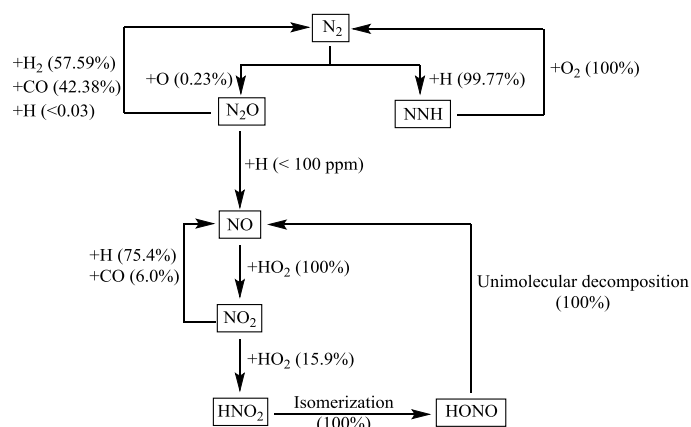
At all of the conditions investigated N_2 is consumed by recombining with either $\dot{H}$ atoms forming NNH (over 99.7%) via R49 ($N_2 + \dot{H}$ (+ M) = NNH (+ M)) or with $\ddot{O}$ atoms forming N_2O (less 0.3%) via R11 ($N_2 + \ddot{O}$ (+M) = N_2O (+M)). Despite the fact that the former pathway consumes most of the N_2, the latter pathway appears to be a dominant channel in producing NO since 100% of the NNH generated from R49 can react with molecular oxygen to re-form N_2 together with the release of $H\ddot{O}_2$ radicals via R50 (NNH + O_2 = N_2 + $H\dot{O}_2$), especially at $\varphi = 0.3$ and 0.75. The N_2O formed from R11 mainly undergoes O-atom abstractions by the fuel molecules via R20 and R51 (N_2O + CO = N_2 + CO_2), resulting in the regeneration of N_2. Only a very small amount of N_2O reacts with $\dot{H}$ atoms via

45

R13 resulting in NO formation. The amount of NO formed less than 100 ppm at $\varphi = 0.3$ but increases to 300 ppm at $\varphi = 0.75$ and to 1.88% at $\varphi = 2.0$. Even through NO has similar formation pathways at different equivalence ratios, there are quite different kinetic mechanisms involved in its consumption at different equivalence ratios. At $\varphi = 0.3$, 100% of NO is converted to NO_2 by reacting with $H\dot{O}_2$ radicals *via* R–7 due to the abundance of $H\dot{O}_2$ radicals present in this lean environment. Most of the NO_2 subsequently reacts with either $\dot{H}$ atoms (75.4%) *via* R5 or with CO (6.0%) *via* R10 to reproduce NO resulting in an inter-conversion of NO into NO_2. Only 15.9% of the NO_2 is further oxidized by $H\dot{O}_2$ radicals *via* R8 forming HNO_2, followed by isomerization to HONO, which finally decomposes to NO and $\dot{O}H$ radicals *via* R–34. However, at $\varphi = 0.75$ NO consumption occurs either by its reaction with $\ddot{O}$ atoms (61.7%) *via* R4 forming NO_2 or by reaction with $\dot{H}$ atoms (38.3%) *via* R25 forming HNO. Both NO_2 and HNO can be converted into NO *via* O-atom abstraction and H-atom abstraction reactions respectively, until they reach an equilibrium concentration. Although the NO consumption pathways are somewhat different at $\varphi = 0.3$ and 0.75, the NO to NO_2 inter-conversion pathways continue to play a dominant role rather than NO to HNO conversion, suggesting that there is a comparable NO consumption rate at both equivalence ratios. Thus, there is a two-fold reason for the higher NO concentration presented at $\varphi = 0.75$, Fig. 17(b). Namely, 1) there is a faster NO formation rate due to the rate of R13 being accelerated due to an increased concentration of $\dot{H}$ atoms generated at $\varphi = 0.75$ and 2) there are similar NO consumption rates due to the dominant role of NO_2 to NO conversion in NO consumption at both equivalence ratios.

At $\varphi = 2.0$, N_2O can be formed by the reaction of NNH with $\ddot{O}$ atoms (100 ppm) *via* R52 (NNH $+ \ddot{O} = N_2O + \dot{H}$) in addition to the direct oxidation of N_2 *via* R11. Likewise, N_2O is mainly consumed by R13 resulting in NO formation. Unlike the case for fuel-lean conditions, a small amount of NNH

(100 ppm) can also contribute to NO formation by recombining with $\dot{H}$ atoms *via* R53 (NNH + $\dot{H}$ (+M) = N_2H_2 (+M)) followed by the reaction of N_2H_2 with $\ddot{O}$ atoms *via* R54 (N_2H_2 + $\ddot{O}$ = NO + NH_2). All (100%) of the NO formed is then converted to HNO *via* R25 due to the relatively high concentration of $\dot{H}$ atoms and low concentrations of $H\dot{O}_2$ radicals and $\ddot{O}$ atoms at fuel-rich conditions. All of the HNO can react back to NO through H-atom abstraction reactions *via* $\dot{H}$ atoms (81.75%) in R26, *via* $\dot{O}H$ radicals (14.56%) in R28 and *via* $\ddot{O}$ atoms (3.69%) in R27. It is worth noting that, despites the seemingly high percentage of NO that is observed at $\varphi = 2.0$, the lower total amount of N_2 at fuel-rich conditions results in a lower rate of formation of N_2O and NNH precursors relative to fuel-lean conditions. Additionally, the reaction rate of R26, which predominantly converts HNO into NO, is essentially unfavorable due to the rate constant being several times lower than that of R25 as well as a higher concentration of H_2 at fuel-rich conditions. As a result, the conversion efficiency of HNO into NO is much slower than that of NO into HNO resulting in a lower rate of NO production.

(a) $\varphi = 0.3$, $p = 30$ atm, $T = 850$ K

+H$_2$ (57.59%)
+CO (42.38%)
+H (<0.03)

+O (0.23%)

N$_2$

+H (99.77%)

+O$_2$ (100%)

N$_2$O

NNH

+H (< 100 ppm)

NO

+H (75.4%)
+CO (6.0%)

+HO$_2$ (100%)

Unimolecular decomposition (100%)

NO$_2$

+HO$_2$ (15.9%)

HNO$_2$ — Isomerization (100%) → HONO

47

(b) $\varphi = 0.75$, $p = 30$ atm, $T = 850$ K

+H$_2$ (75.76%)
+CO (23.47)
+H (0.73)

N$_2$

+O (0.25%)

+H (99.75%)

+O$_2$ (100%)

N$_2$O

NNH

+H (300 ppm)

NO

+O$_2$ (87.5%)
+H (6.7%)
+OH (4.9%)

+H (38.3%)

+O (61.7%)

+H (96.1%)
+CO (1.9%)
+O (1.6%)

HNO

NO$_2$

(c) $\varphi = 2.0$, $p = 30$ atm, $T = 850$ K

+H$_2$ (73.76%)
+H (15.77)
+CO (8.48%)
+O (0.08)

N$_2$

+O (0.28%)

+O (100 ppm)

+H (99.72%)

+O$_2$ (99.5%)
+H (<0.4%)
+OH (0.06%)
+O (0.02%)

N$_2$O

NNH

+H (1.88%)
+O (300 ppm)

+H (100 ppm)

+H (77.71%)
+O (9.59%)
+OH (3.22%)

+O (6.3%)

NO

N$_2$H$_2$

+H (81.75%)
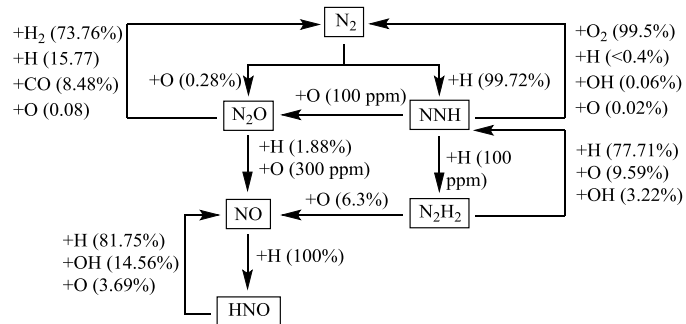+OH (14.56%)
+O (3.69%)

+H (100%)

HNO

Fig. 18. Flux analysis of NO formations for 50% H$_2$/50% CO in air mixtures at 30 atm under different equivalence ratios. The reaction time corresponds to 20% of hydrogen consumption. (a) $\varphi = 0.3$; (b) $\varphi = 0.75$; (c) $\varphi = 2.0$.

5. Conclusions

In *this study*, we have developed a detailed kinetic mechanism to describe the hydrogen/NO$_x$ and syngas/NO$_x$ systems. Critically important reactions associated with the Zeldovich mechanism, the N/O sub-mechanism involving nitrogen dioxide, nitrous oxide, nitrogen trioxide, the H/N/O sub-mechanism involving nitroxyl isomer, nitrous acid isomers, and nitric acid isomers, and the NH$_3$ mechanism have been described. Additionally, some missing reaction pathways involving HOĊO kinetics of the CO chemistry sub-mechanism have also been considered in the current model. The rate constants used for these important reactions associated with the pyrolysis and oxidation of each NOx sub-mechanism have been selected by comparison with literature values and integrating the latest published values. We have optimized several rate constants that had a large uncertainty by

testing against the experimental data but did not further modify the rate constants obtained from either directly experimental measurements or high-level theoretically calculation in the literature.

The ability of the mechanism developed in *this study* to simulate a wide-range of experimental data for various reaction systems including $H_2/O_2/N_2$, N_2O pyrolysis, H_2/N_2O, $H_2/NO_x/O_2$, CO/ $H_2O/$ NO_x/O_2, $H_2/CO/NO_x/O_2$ and the $H_2/CO/H_2O/NO_x/O_2$ system. A large number of experimental data including 104 shock tube data sets, 87 JSR data sets, 87 FR data sets and 6 laminar flame speed data sets over 3000 experimental points were used. Overall, the current model gives a satisfactory representation of the experimental data over a wide range of conditions for each of the selected data sets considered here. Through the comparisons of the proposed mechanism and a selection of available literature mechanisms, we found that each literature mechanism performed well for certain systems but exhibited relatively noticeable deviations compared to others. It is suggested that the reason for the different simulation results by different mechanisms may be three-fold: a) different hydrogen/CO chemical kinetics, b) different NOx chemistry and c) different thermochemistry for the species. Therefore, only updating one of these either the kinetic parameters as part of the sub-mechanisms or the thermochemistry of the species may not result in a high-fidelity model.

An open question proposed by Dayma and Dagaut [28] in 2008 was that the kinetic model was not able to capture the fall-off behavior of NO concentration with increasing temperatures at low pressures (1.0 atm) and this issue also pertains to the current literature models. We found that HON chemistry appears to be a promising way to resolve this problem through R32: $HON + \dot{H} = \dot{O}H +$ NH in competition for $\dot{H}$ atoms with R26 ($HNO + \dot{H} = NO + H_2$) which reduces the rate of NO formation at low pressures. However, further experimental and/or theoretical research of HON chemistry is recommended to better explore its kinetic role in combustion mechanisms.

The proposed mechanism was also used to simulate NO formation at practical gas-turbine conditions. We found that a change in pressure does not effectively control the formation of NO during fuel oxidation/ignition rather that changes in temperature and equivalence ratio appear to provide a better strategy. By contrast, controlling the equivalence ratio appears to be a more efficient way of controlling NO formation, because the kinetic pathways that lead to its formation/consumption are more sensitivity to the variations in equivalence ratio.

References

[1] S. Bhaduri, B. Berger, M. Pochet, H. Jeanmart, F. Contino, Fuel Processing Technology, 157 (2017) 52-58.

[2] J. Wünning, J. Wünning, Progress in Energy and Combustion Science, 23 (1997) 81-94.

[3] H. Omidvarborna, A. Kumar, D.-S. Kim, Fuel Processing Technology, 140 (2015) 113-118.

[4] R. Burch, J. Breen, F. Meunier, Applied Catalysis B: Environmental, 39 (2002) 283-303.

[5] L. Muzio, G. Quartucy, J. Cichanowiczy, International Journal of Environment and Pollution, 17 (2002) 4-30.

[6] T. Yamamoto, M. Okubo, K. Hayakawa, K. Kitaura, IEEE Transactions on Industry applications, 37 (2001) 1492-1498.

[7] X. Tauzia, A. Maiboom, S.R. Shah, Energy, 35 (2010) 3628-3639.

[8] O. Mathieu, A. Levacque, E. Petersen, Proceedings of the Combustion Institute, 34 (2013) 633-640.

[9] C.L. Rasmussen, J. Hansen, P. Marshall, P. Glarborg, International Journal of Chemical Kinetics, 40 (2008) 454-480.

[10] M. Mueller, R. Yetter, F. Dryer, International Journal of Chemical Kinetics, 31 (1999) 705-724.

[11] J.-B. Masurier, F. Foucher, G. Dayma, P. Dagaut, Proceedings of the Combustion Institute, 35 (2015) 3125-3132.

[12] F. Contino, F. Foucher, P. Dagaut, T. Lucchini, G. D'Errico, C. Mounaïm-Rousselle, Combustion and Flame, 160 (2013) 1476-1483.

[13] A. Konnov, Combustion and Flame, 156 (2009) 2093-2105.

[14] L. Moskaleva, M. Lin, Proceedings of the Combustion Institute, 28 (2000) 2393-2401.

[15] S.F. Ahmed, J. Santner, F.L. Dryer, B. Padak, T.I. Farouk, Energy & Fuels, 30 (2016) 7691-7703.

[16] O. Mathieu, M. Kopp, E. Petersen, Proceedings of the Combustion Institute, 34 (2013) 3211-3218.

[17] C.T. Bowman, Combustion Science and Technology, 3 (1971) 37-45.

[18] O. Mathieu, A. Levacque, E. Petersen, International Journal of Hydrogen Energy, 37 (2012) 15393-15405.

[19] R. Mével, S. Javoy, F. Lafosse, N. Chaumeix, G. Dupré, C.-E. Paillard, Proceedings of the Combustion Institute, 32 (2009) 359-366.

[20] S. Javoy, R. Mével, C. Paillard, International Journal of Chemical Kinetics, 41 (2009) 357-375.

[21] A. Zuev, A.Y. Starikovskii, Sov. J. Chem. Phys, 10 (1992) 80-99.

[22] I. Kosarev, S. Starikovskaia, A.Y. Starikovskii, Combustion and Flame, 151 (2007) 61-73.

[23] H. Henrici, S. Bauer, The Journal of Chemical Physics, 50 (1969) 1333-1342.

[24] Y. Hidaka, H. Takuma, M. Suga, The Journal of Physical Chemistry, 89 (1985) 4903-4905.

[25] K.M. Pamidimukkala, G.B. Skinner, The Journal of Chemical Physics, 76 (1982) 311-315.

[26] A. Borisov, G. Skachkov, Kinet. Catalysis, 13 (1972) 42-47.

[27] M. Kopp, M. Brower, O. Mathieu, E. Petersen, F. Güthe, Applied Physics B, 107 (2012) 529-538.

[28] G. Dayma, P. Dagaut, Combustion Science and Technology, 178 (2006) 1999-2024.

[29] P. Dagaut, A. Nicolle, Combustion and Flame, 140 (2005) 161-171.

[30] P. Dagaut, F. Lecomte, J. Mieritz, P. Glarborg, International Journal of Chemical Kinetics, 35 (2003) 564–575.

[31] M. Abian, M.U. Alzueta, P. Glarborg, International Journal of Chemical Kinetics, 47 (2015) 518-532.

[32] P. Glarborg, D. Kubel, P.G. Kristensen, J. Hansen, K. Dam-Johansen, Combustion Science and Technology, 110 (1995) 461-485.

[33] R. Mével, F. Lafosse, N. Chaumeix, G. Dupré, C.-E. Paillard, International Journal of Hydrogen Energy, 34 (2009) 9007-9018.

[34] S. Bane, R. Mével, S. Coronel, J. Shepherd, International Journal of Hydrogen Energy, 36 (2011) 10107-10116.

[35] P. Dagaut, F. Lecomte, S. Chevailler, M. Cathonnet, Combustion Science and Technology, 139 (1998) 329-363.

[36] D. Baulch, C. Cobos, R. Cox, P. Frank, G. Hayman, T. Just, J. Kerr, T. Murrells, M. Pilling, J. Troe, Journal of Physical and Chemical Reference Data, 23 (1994) 847-848.

[37] W. Tsang, Journal of Physical and Chemical Reference Data, 21 (1992) 753-791.

[38] W. Tsang, J.T. Herron, Journal of Physical and Chemical Reference Data, 20 (1991) 609-663.

[39] S.J. Klippenstein, L.B. Harding, P. Glarborg, J.A. Miller, Combustion and Flame, 158 (2011) 774-789.

[40] J. Chai, C.F. Goldsmith, Proceedings of the Combustion Institute, (2016).

[41] A. Frassoldati, T. Faravelli, E. Ranzi, International Journal of Hydrogen Energy, 32 (2007) 3471-3485.

[42] G.P. Smith, D.M. Golden, M. Frenklach, N.W. Moriarty, B. Eiteneer, M. Goldenberg, C.T. Bowman, R.K. Hanson, S. Song, W.C. Gardiner Jr, URL: http://www. me. berkeley. edu/gri_mech, 51 (1999) 55.

[43] U.o.C.a.S. Diego.

[44] J.A. Miller, C.T. Bowman, Progress in Energy and Combustion Science, 15 (1989) 287-338.

[45] F. Deng, F. Yang, P. Zhang, Y. Pan, J. Bugler, H.J. Curran, Y. Zhang, Z. Huang, Fuel, 181 (2016) 188-198.

[46] J.F. Roesler, R.A. Yetter, F.L. Dryer, Combustion and Flame, 100 (1995) 495-504.

[47] J. Bromly, F. Barnes, P. Nelson, B. Haynes, International Journal of Chemical Kinetics, 27 (1995) 1165-1178.

[48] A.A. Konnov, J.D. Ruyck, Combustion Science and Technology, 168 (2001) 1-46.

[49] A. Konnov, G. Colson, J. De Ruyck, Fuel, 80 (2001) 49-65.

[50] J.W. Bozzelli, A.M. Dean, International Journal of Chemical Kinetics, 27 (1995) 1097-1109.

[51] M. Slack, A. Grillo, NASA Report CR-2896, (1977).

[52] G.M. Watson, J.D. Munzar, J.M. Bergthorson, Energy & Fuels, 27 (2013) 7031-7043.

[53] Z. Tian, Y. Li, L. Zhang, P. Glarborg, F. Qi, Combustion and Flame, 156 (2009) 1413-1426.

[54] M.P. Burke, M. Chaos, Y. Ju, F.L. Dryer, S.J. Klippenstein, International Journal of Chemical Kinetics, 44 (2012) 444-474.

[55] H. Hashemi, J.M. Christensen, S. Gersen, P. Glarborg, Proceedings of the Combustion Institute, 35 (2015) 553-560.

[56] W.K. Metcalfe, S.M. Burke, S.S. Ahmed, H.J. Curran, International Journal of Chemical Kinetics, 45 (2013) 638-675.

[57] A. Kéromnès, W.K. Metcalfe, K.A. Heufer, N. Donohoe, A.K. Das, C.-J. Sung, J. Herzler, C. Naumann, P. Griebel, O. Mathieu, Combustion and Flame, 160 (2013) 995-1011.

[58] J. Bugler, K.P. Somers, J.M. Simmie, F. Güthe, H.J. Curran, The Journal of Physical Chemistry A, 120 (2016) 7192-7197.

[59] P. Dagaut, P. Glarborg, M.U. Alzueta, Progress in Energy and Combustion Science, 34 (2008) 1-46.

[60] R.E. Weston Jr, T.L. Nguyen, J.F. Stanton, J.R. Barker, The Journal of Physical Chemistry A, 117 (2013) 821-835.

[61] T.L. Nguyen, B.C. Xue, R.E. Weston Jr, J.R. Barker, J.F. Stanton, The Journal of Physical Chemistry Letters, 3 (2012) 1549-1553.

[62] H.-G. Yu, J.T. Muckerman, The Journal of Physical Chemistry A, 110 (2006) 5312-5316.

[63] H.-G. Yu, J.T. Muckerman, J.S. Francisco, The Journal of Physical Chemistry A, 109 (2005) 5230-5236.

[64] H.-G. Yu, J.S. Francisco, The Journal of Chemical Physics, 128 (2008) 244315.

[65] H.-G. Yu, J.T. Muckerman, J.S. Francisco, The Journal of Chemical Physics, 127 (2007) 094302.

[66] H.-G. Yu, G. Poggi, J.S. Francisco, J.T. Muckerman, The Journal of Chemical Physics, 129 (2008) 214307-214307.

[67] H.-G. Yu, J.S. Francisco, The Journal of Physical Chemistry A, 113 (2009) 3844-3849.

[68] J.S. Francisco, J.T. Muckerman, H.-G. Yu, Accounts of Chemical Research, 43 (2010) 1519-1526.

[69] G. Poggi, J.S. Francisco, The Journal of Chemical Physics, 130 (2009) 124306.

[70] G. Poggi, J.S. Francisco, The Journal of Chemical Physics, 120 (2004) 5073-5080.

[71] Y.B. Zeldovich, Acta Physicochim. URSS, 21 (1946) 577-628.

[72] D. Baulch, C. Bowman, C. Cobos, R. Cox, T. Just, J. Kerr, M. Pilling, D. Stocker, J. Troe, W. Tsang, Journal of Physical and Chemical Reference Data, 34 (2005) 757-1397.

[73] S. Klippenstein, L. Harding, B. Ruscic, R. Sivaramakrishnan, N. Srinivasan, M.-C. Su, J. Michael, The Journal of Physical Chemistry A, 113 (2009) 10241-10259.

[74] K. Becker, W. Groth, D. Kley, Zeitschrift für Naturforschung A, 24 (1969) 1280-1281.

[75] W. Wilson, The Journal of Chemical Physics, 46 (1967) 2017-2018.

[76] A.S. Vlastaras, C. Winkler, Canadian Journal of Chemistry, 45 (1967) 2837-2840.

[77] M. Clyne, B. Thrush, in: Proceedings of the Royal Society of London A: Mathematical, Physical and Engineering Sciences, The Royal Society, 1961, pp. 259-273.

[78] J.A. Miller, M.C. Branch, W.J. McLean, D.W. Chandler, M.D. Smooke, R.J. Kee, in: Symposium (International) on Combustion, Elsevier, 1985, pp. 673-684.

[79] M.J. Howard, I.W. Smith, Journal of the Chemical Society, Faraday Transactions 2: Molecular and Chemical Physics, 77 (1981) 997-1008.

[80] T. Ko, A. Fontijn, The Journal of Physical Chemistry, 95 (1991) 3984-3987.

[81] C.J. Howard, Journal of the American Chemical Society, 102 (1980) 6937-6941.

[82] L.M. Avallone, Journal of Photochemistry and Photobiology A: Chemistry, 157 (2003) 231-236.

[83] P.P. Bemand, M.A. Clyne, R.T. Watson, Journal of the Chemical Society, Faraday Transactions 2: Molecular and Chemical Physics, 70 (1974) 564-576.

[84] E. Estupinan, J. Nicovich, P. Wine, The Journal of Physical Chemistry A, 105 (2001) 9697-9703.

[85] R. Geers-Müller, F. Stuhl, Chemical Physics Letters, 135 (1987) 263-268.

[86] B.A. Shiekh, D. Kaur, B. Seth, S. Mahajan, Chemical Physics Letters, 662 (2016) 244-249.

[87] P. Glarborg, M. Alzueta, K. Kjærgaard, K. Dam-Johansen, Combustion and Flame, 132 (2003) 629-638.

[88] J. Park, N.D. Giles, J. Moore, M. Lin, The Journal of Physical Chemistry A, 102 (1998) 10099-10105.

[89] H. Freund, H. Palmer, International Journal of Chemical Kinetics, 9 (1977) 887-905.

[90] D. Milks, T. Adams, R. Matula, Combustion Science and Technology, 19 (1979) 151-159.

[91] S.K. Ross, J.W. Sutherland, S.-C. Kuo, R.B. Klemm, The Journal of Physical Chemistry A, 101 (1997) 1104-1116.

[92] W.D. Breshears, The Journal of Physical Chemistry, 99 (1995) 12529-12535.

[93] M. Röhrig, E.L. Petersen, D.F. Davidson, R.K. Hanson, International Journal of Chemical Kinetics, 28 (1996) 599-608.

[94] A.H. Chang, D.R. Yarkony, The Journal of Chemical Physics, 99 (1993) 6824-6831.

[95] A. Zuev, A. Starikovskii, Khim. Fiz., 10 (1991) 52-63.

[96] R. Mevel, F. Lafosse, L. Catoire, N. Chaumeix, G. Dupre, C.-E. Paillard, Combustion Science and Technology, 180 (2008) 1858-1875.

[97] P. Marshall, A. Fontijn, C.F. Melius, The Journal of Chemical Physics, 86 (1987) 5540-5549.

[98] A.M. Dean, J.W. Bozzelli, Combustion chemistry of nitrogen, in: Gas-phase combustion chemistry, Springer, 2000, pp. 125-341.

[99] D. Davidson, M. DiRosa, A. Chang, R. Hanson, Shock Waves, (1992) 813-818.

[100] N.E. Meagher, W.R. Anderson, The Journal of Physical Chemistry A, 104 (2000) 6013-6031.

[101] A. Fontijn, A. Goumri, A. Fernandez, W.R. Anderson, N.E. Meagher, The Journal of Physical Chemistry A, 104 (2000) 6003-6012.

[102] A. Mebel, M. Lin, K. Morokuma, C. Melius, International Journal of Chemical Kinetics, 28 (1996) 693-703.

[103] J. Hahn, K. Luther, J. Troe, Physical Chemistry Chemical Physics, 2 (2000) 5098-5104.

[104] L.B. Harding, H. Stark, J. Troe, V.G. Ushakov, Physical Chemistry Chemical Physics, 1 (1999) 63-72.

[105] R. Atkinson, D. Baulch, R. Cox, R. Hampson, J. Kerr, J. Troe, Atmospheric Environment. Part A. General Topics, 26 (1992) 1187-1230.

[106] E. Becker, M. Rahman, R. Schindler, Berichte der Bunsengesellschaft für physikalische Chemie, 96 (1992) 776-783.

[107] P. Glarborg, M. Østberg, M.U. Alzueta, K. Dam-Johansen, J.A. Miller, in: Symposium (International) on Combustion, Elsevier, 1998, pp. 219-226.

[108] M.T. Allen, R.A. Yetter, F.L. Dryer, Combustion and Flame, 112 (1998) 302-311.

[109] P.S. Riley, B. Cosic, A. Fontijn, International Journal of Chemical Kinetics, 35 (2003) 374-380.

[110] M.R. Soto, M. Page, The Journal of Chemical Physics, 97 (1992) 7287-7296.

[111] H.M.T. Nguyen, S. Zhang, J. Peeters, T.N. Truong, M.T. Nguyen, Chemical Physics Letters, 388 (2004) 94-99.

[112] M.R. Soto, M. Page, M.L. McKee, Chemical Physics, 153 (1991) 415-426.

[113] S. Inomata, N. Washida, The Journal of Physical Chemistry A, 103 (1999) 5023-5031.

[114] A. Mebel, M. Lin, K. Morokuma, International Journal of Chemical Kinetics, 30 (1998) 729-736.

[115] N. Faßheber, M.C. Schmidt, G. Friedrichs, Proceedings of the Combustion Institute, (2016).

[116] D. Fulle, H. Hamann, H. Hippler, J. Troe, Journal of Chemical Physics, 108 (1998) 5391-5397.

[117] R. Atkinson, D. Baulch, R. Cox, J. Crowley, R. Hampson, R. Hynes, M. Jenkin, M. Rossi, J. Troe, Atmospheric Chemistry and Physics, 4 (2004) 1467-1738.

[118] C.-C. Hsu, M. Lin, A. Mebel, C. Melius, The Journal of Physical Chemistry A, 101 (1997) 60-66.

[119] W. Xia, M. Lin, PhysChemComm, 3 (2000) 71-78.

[120] J.B. Burkholder, A. Mellouki, R. Talukdar, A. Ravishankara, International Journal of Chemical Kinetics, 24 (1992) 711-725.

[121] D.-Q. Wang, J.-L. Li, X.-R. Huang, C.-Y. Geng, C.-C. Sun, Journal of Molecular Structure: THEOCHEM, 847 (2007) 10-22.

[122] X. Lu, J. Park, M. Lin, The Journal of Physical Chemistry A, 104 (2000) 8730-8738.

[123] A. Mebel, M. Lin, C. Melius, The Journal of Physical Chemistry A, 102 (1998) 1803-1807.

[124] S.-y. Takane, T. Fueno, Theoretica Chimica Acta, 87 (1994) 431-439.

[125] X. Lu, R.N. Musin, M. Lin, The Journal of Physical Chemistry A, 104 (2000) 5141-5148.

[126] C. Eckart, Physical Review, 35 (1930) 1303.

[127] R. Asatryan, J.W. Bozzelli, J.M. Simmie, International Journal of Chemical Kinetics, 39 (2007) 378-398.

[128] J.r. Troe, The Journal of Physical Chemistry A, 116 (2012) 6387-6393.

[129] J. Troe, International Journal of Chemical Kinetics, 33 (2001) 878-889.

[130] H. Hippler, S. Nasterlack, F. Striebel, Physical Chemistry Chemical Physics, 4 (2002) 2959-2964.

[131] W. Xia, M. Lin, Journal of Chemical Physics, 114 (2001) 4522-4532.

[132] S.S. Brown, R.K. Talukdar, A. Ravishankara, The Journal of Physical Chemistry A, 103 (1999) 3031-3037.

[133] S.S. Brown, J.B. Burkholder, R.K. Talukdar, A. Ravishankara, The Journal of Physical Chemistry A, 105 (2001) 1605-1614.

[134] G. Poskrebyshev, P. Neta, R.E. Huie, Journal of Geophysical Research: Atmospheres, 106 (2001) 4995-5004.

[135] R. Atkinson, D. Baulch, R. Cox, R. Hampson Jr, J. Kerr, M. Rossi, J. Troe, Journal of Physical and Chemical Reference Data, 26 (1997) 1329-1499.

[136] J.J. Lamb, M. Mozurkewich, S.W. Benson, The Journal of Physical Chemistry, 88 (1984) 6441-6448.

[137] O. Mathieu, E.L. Petersen, Combustion and Flame, 162 (2015) 554-570.

[138] A. Borisov, V. Zamanskii, G. Skachkov, Kinet. Catalysis, 13 (1978) 42-47.